ISSN 0256-4637
VOLUME 39 NUMBER 2 APRIL-JUNE 2017

Journal of Pure and Applied

Ultrasonics

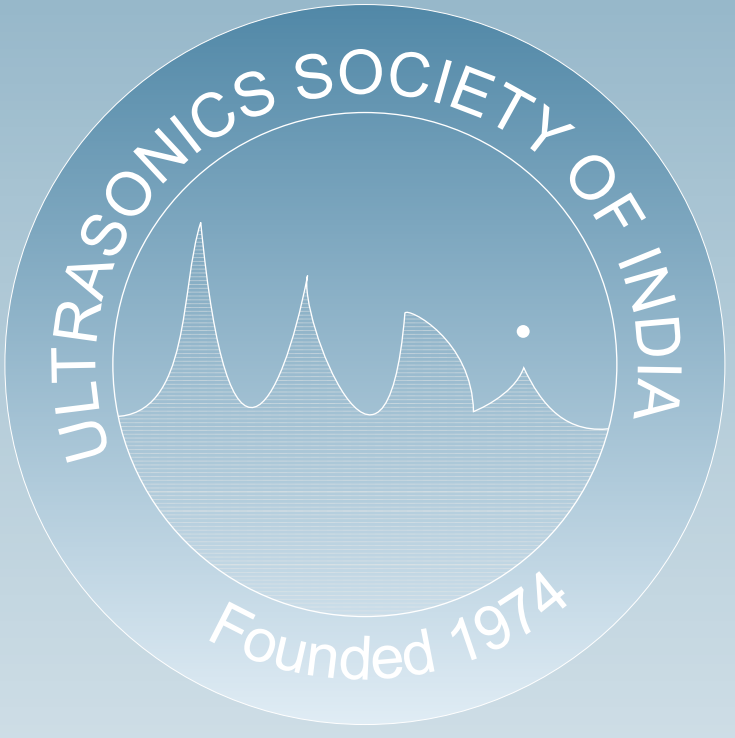

Website : www.ultrasonicsindia.org

A Publication of Ultrasonics Society of India

A Quarterly Publication of Ultrasonics Society of India

Journal of Pure and Applied

Ultrasonics

No. 2	Volume 39	April-June 2017

SUBSCRIPTION (postage paid)

Single	Rs. 750/-	US$ 60/-
Annual	Rs. 3000/-	US$ 250/-
USI *members*	Free	

The submission of papers and all other correspondence regarding the Journal may please be addressed to :

Publication Secretary
Journal of Pure and Applied Ultrasonics
C/o Ultrasonics Society of India
CSIR-National Physical Laboratory
Dr. K.S. Krishnan Road, New Delhi-110012
publicationsecretary.usi@gmail.com
www.ultrasonicsindia.org

ISSN 0256–4637

Journal of Pure and Applied Ultrasonics

VOLUME 39 NUMBER 2 APRIL–JUNE 2017

CONTENTS

(Authors have stated that the papers have not been published elsewhere)

Website : www.ultrasonicsindia.org

A Publication of — Ultrasonics Society of India

J. Pure Appl. Ultrason. 39 (2017) pp. 35-39

Molecular interactions in binary liquid mixtures – an ultrasonic study

J.V. Srinivasu[1,*], K. Narendra[2], Ch. Kavitha[2], T. Srinivasa Krishna[3] and B. Subba Rao[4]

[1]Department of Basic Science,Shri Vishnu Engineering College for Women, Bhimavaram-534202, India
[2]Department of Physics, V.R. Siddhartha Engineering College, Vijayawada-520007, India
[3]Department of Physics, Rayalaseema University, Kurnool-518002, India
[4]Department of Physics, VSR & NVR College, Tenali-522201, India
*E-mail: srinivas.jaddu@gmail.com

The densities and speed of sound of the binary mixture1, 4-butanediol with γ-picoline have been measured over the entire composition range in the temperature range 303.15 to 318.15 K at ambient pressure. From the experimental data, the excess molar volume, excess isentropic compressibility and excess molarisentropic compressibility have been calculated. The excess partial molar volume, excess partial molar isentropic compressions and their limiting values at infinite dilution have also been calculated. Excess parameters are fitted to the Redlich-Kister polynomial equation. The variations of these parameters with composition and temperature are discussed in terms of intermolecular interactions.

Keywords: Binary mixture, speed of sound, excess properties, molecular interactions.

Introduction

The thermophysical, thermodynamic and bulk properties of binary mixtures are studied for many reasons, specifically in light of the fact of their ability to provide information about the nature and extent of molecular interactions in the liquid state. Alkanediols are chemically very similar to alcohols and the hydration properties have been observed for these compounds by several authors[1-2]. Butanediols are four carbon diols that have many industrial and biological applications[3]. 1, 4-butanediol (BD) is a clear viscous liquid, which is miscible with water and most polar organic solvents. However, in the case of diols, due to the presence of two -OH groups in the molecule, the dielectric properties and the dipole moments of the diols strongly influenced by the location of -OH groups (the separation of the two -OH groups along the carbon skeleton), molecular conformations and molecular flexibility. Moreover, formation of network structure in diols, due to the molecular association, is a well-known phenomenon and makes it suitable as a useful chemical intermediate in the manufacture of many chemical products.

γ – picoline refers to one of methyl pyridine isomers, and colourless liquid at room temperature and pressure.It is miscible with water and volatile organic solvents. γ-picoline is used in water proofing agents for fabrics, synthesis of pharmaceuticals, rubber accelerators, pesticides, manufacture of isonicotinic acid and derivatives.

The excess properties are necessary for the design and calculation of the chemical engineering process involving substance separation, heat transfer, mass transfer and fluid flow[4]. The information about the excess properties of liquid mixtures containing 1, 4-BD and γ-picoline, and their dependence on composition and temperature constitute are very important fundamental data owing to their applications in different fields. To date, numerous studies havebeen centered on binary or ternary systems consisted of H-bond containing chemicals such as alcohols with non-polar or polar solvents[5-7]. With these studies, some important factors responsible for the positive or negative deviations for binary polar-polar or non-polar-polar systems have been discussed. However, a survey of the literature[8-11] reveals that very few reports have been made on the excess parameters for binary

solutions of 1, 4-BD. To the best of our knowledge, literature survey reveals that no studies have been reported till now pertaining to thermodynamic properties of 1, 4-BD with γ-picoline.

These mixtures are very interesting from the experimental as well as theoretical point of view because 1, 4-BD and γ-picoline are polar as indicated by their dipole moments and their dielectric constants ($\mu_{1,4\text{–BD}}$ =2.58 D, $\varepsilon_{1,4\text{–BD}}$ = 30.2 and μ_{picoline} = 1.96 D, $\varepsilon_{\text{picoline}}$ = 13.5)[12].

Hence, the present study will be useful in understanding the competitive role of hydrogen bonding (both intra-and intermolecular) and the nonspecific interactions and structural effects. These considerations prompted us to measure densities, speeds of sound and excess molar properties of binary mixture 1, 4-BD+γ-picoline mixture.

Experimental

The density and speed of sound was measured by using pycnometer and ultrasonic interferometer operating at 2 MHz and the experimental procedure along with the formulas used to determine the excess properties were given in our previous paper[13].

Results and Discussion

Densities and speeds of sound of binary mixtures consisting of 1, 4-BD with γ-picoline has been determined experimentally at four different temperatures, *viz.*, 303.15-318.15 K at atmospheric pressure 0.1 MPa, and

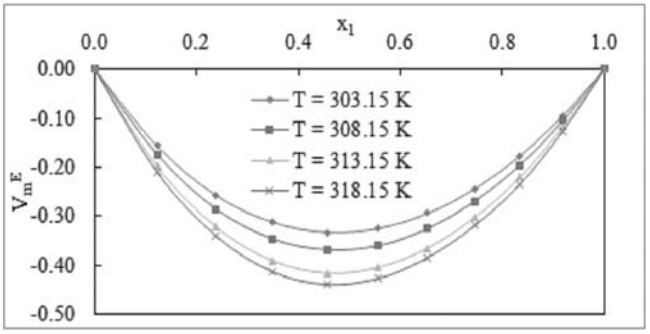

Fig. 1 Variation of V_m^E with mole fraction of 1, 4-BD.

Table 1 – Values of u, ρ, V_m^E, κ_s^E and $K_{s,m}^E$ at different temperatures.

x_1	303.15 K					308.15 K				
	u	ρ	V_m^E	κ_s^E	$K_{s,m}^E$	u	ρ	V_m^E	κ_s^E	$K_{s,m}^E$
0.0000	1410.6	0.9459	0.0000	0.0000	0.0000	1390.1	0.9406	0.0000	0.0000	0.0000
0.1224	1432.9	0.9546	-0.1561	-0.1719	-0.1755	1413.6	0.9497	-0.173	-0.1920	-0.1971
0.2389	1454.1	0.9625	-0.2572	-0.3081	-0.3097	1436.1	0.9581	-0.2849	-0.3279	-0.3319
0.3498	1474.3	0.9699	-0.3119	-0.3743	-0.3721	1457.4	0.9658	-0.3456	-0.3927	-0.3931
0.4556	1493.4	0.9767	-0.3320	-0.4057	-0.3985	1477.7	0.9729	-0.3674	-0.4200	-0.4154
0.5566	1511.6	0.9831	-0.3242	-0.3986	-0.3873	1496.9	0.9795	-0.3593	-0.4116	-0.4026
0.6531	1528.9	0.9891	-0.2937	-0.3616	-0.3477	1515.2	0.9857	-0.3246	-0.3749	-0.3626
0.7455	1545.4	0.9947	-0.2439	-0.2894	-0.2759	1532.6	0.9915	-0.2690	-0.3038	-0.2911
0.8339	1561.0	0.9999	-0.1771	-0.2000	-0.1891	1549.1	0.9970	-0.1956	-0.2213	-0.2099
0.9187	1576.0	1.0048	-0.0941	-0.1026	-0.0962	1564.9	1.0020	-0.1043	-0.1196	-0.1122
1.0000	1590.4	1.0094	0.0000	0.0000	0.0000	1580.5	1.0068	0.0000	0.0000	0.0000
x_1	313.15 K					318.15 K				
0.0000	1365.3	0.9342	0.0000	0.0000	0.0000	1345.5	0.9296	0.0000	0.0000	0.0000
0.1224	1390.6	0.9438	-0.1975	-0.2063	-0.2139	1371.7	0.9394	-0.2091	-0.2240	-0.2334
0.2389	1414.7	0.9527	-0.3216	-0.3376	-0.3454	1396.5	0.9485	-0.3400	-0.3493	-0.3597
0.3498	1437.5	0.9608	-0.3901	-0.4008	-0.4054	1420.0	0.9567	-0.4127	-0.4157	-0.4229
0.4556	1459.3	0.9683	-0.4148	-0.4286	-0.4282	1442.4	0.9644	-0.4383	-0.4405	-0.4426
0.5566	1479.9	0.9753	-0.4034	-0.4218	-0.4162	1463.6	0.9715	-0.4261	-0.4313	-0.4281
0.6531	1499.5	0.9818	-0.3642	-0.3806	-0.3714	1483.9	0.9781	-0.3836	-0.3941	-0.3864
0.7455	1518.2	0.9879	-0.3018	-0.3170	-0.3059	1503.1	0.9843	-0.3185	-0.3336	-0.3232
0.8339	1535.9	0.9936	-0.2203	-0.2295	-0.2192	1521.3	0.9901	-0.2347	-0.2480	-0.2377
0.9187	1552.8	0.9988	-0.1174	-0.1275	-0.1204	1538.7	0.9954	-0.1254	-0.1411	-0.1335
1.0000	1569.2	1.0038	0.0000	0.0000	0.0000	1555.2	1.0004	0.0000	0.0000	0.0000

given in Table1. The excess molar volume (V_m^E) values are observed to be negative over the entire mole fraction range with the values being highest (negative) in the equimolar region. By close perusal of Fig. 1, the excess molar volume values show an increase, more negative, with increase in temperature range 303.15 - 318.15 *K*. Negative V_m^E values are stemming from interactions between unlike molecules[14].

(i) 1, 4-BD and γ-picoline exist as self associated molecules (ii) there is an interaction between π-electron spilling over nitrogen and oxygen atom (-OH) of 1, 4-BD and π-electron cloud of Py or γ-picolines; (iii) interactions between 1, 4-BD and γ-picolines of (*i* + *j*) binary mixtures then rupture self association to yield their respective monomers which in turn enhance randomness; (iv) monomers of (*i*) and (*j*) then undergo specific interactions to form *i:j* molecular entity and give non-random structure; and (v) there is steric repulsion between 1, 4-BD and γ-picolines.

The values of excess isentropic compressibilities, κ_s^E, for the system over the entire concentration range are seen to be negative (Fig. 2) with all of them exhibiting an increase in the values (negative) with increase in the temperature.

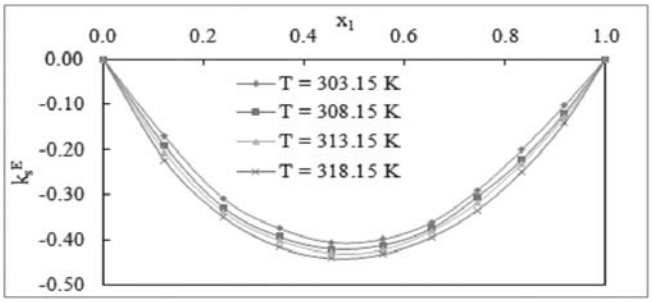

Fig. 2 Variation of κ_s^E with mole fraction of 1, 4-BD.

The excess isentropic compressibilities, κ_s^E have been regularly investigated to study the nature and extent of intermolecular interactions[15,16]. The behavior of $K_{s,m}^E$, with 1, 4-BD concentration and temperature is shown in Fig. 3.

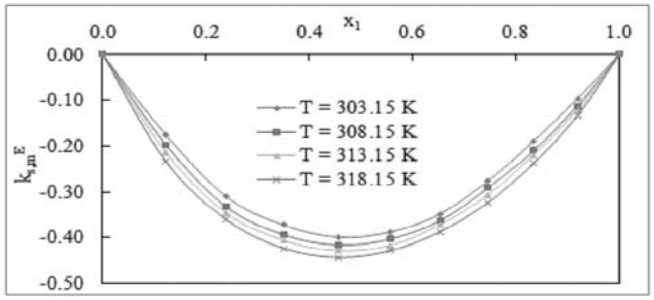

Fig. 3 Variation of $K_{s,m}^E$ with mole fraction of 1, 4-BD.

The $K_{s,m}^E$, were negative for the studied binary systems and decreases with increasing temperature. The possible accommodation of small solvent molecules in free volumes of 1, 4-BD and specific interaction within binary mixtures support negative behavior of $K_{s,m}^E$. As concentration of 1, 4-BD in binary mixtures increases, specific interaction increases leading to decrease in compressibility.

The values of excess partial molar properties, $\overline{V}_{m,1}^E$ and $\overline{V}_{m,2}^E$, of 1, 4-BD and γ-picoline at infinite dilution were calculated as function of mole fraction, x_1 of 1, 4-BD. The $\overline{V}_{m,1}^E$ and $\overline{V}_{m,2}^E$ values were given in Table 2.

Table 2 – Values of $\overline{V}_{m,1}^E$ and $\overline{V}_{m,2}^E$ at different temperatures.

x_1	303.15 K		308.15 K		313.15 K		318.15 K	
	$\overline{V}_{m,1}^E$	$\overline{V}_{m,2}^E$	$\overline{V}_{m,1}^E$	$\overline{V}_{m,2}^E$	$\overline{V}_{m,1}^E$	$\overline{V}_{m,2}^E$	$\overline{V}_{m,1}^E$	$\overline{V}_{m,2}^E$
0.0000	-1.4751	0.0000	-1.6473	0.0000	-1.9131	0.0000	-2.0287	0.0000
0.1224	-1.1513	-0.0173	-1.2769	-0.0192	-1.4601	-0.0212	-1.5457	-0.0223
0.2389	-0.8656	-0.0661	-0.9581	-0.0732	-1.0877	-0.0816	-1.1523	-0.0858
0.3498	-0.6260	-0.1433	-0.6935	-0.1587	-0.7858	-0.1773	-0.8337	-0.1861
0.4556	-0.4330	-0.2472	-0.4808	-0.2730	-0.5451	-0.3048	-0.5791	-0.3195
0.5566	-0.2831	-0.3756	-0.3151	-0.4135	-0.3577	-0.4610	-0.3801	-0.4833
0.6531	-0.1710	-0.5252	-0.1906	-0.5773	-0.2165	-0.6433	-0.2296	-0.6760
0.7455	-0.0911	-0.6919	-0.1016	-0.7607	-0.1153	-0.8492	-0.1218	-0.8969
0.8339	-0.0386	-0.8705	-0.0430	-0.9595	-0.0485	-1.0765	-0.0509	-1.1460
0.9187	-0.0093	-1.0549	-0.0103	-1.1689	-0.0115	-1.3232	-0.0119	-1.4241
1.0000	0.0000	-1.2384	0.0000	-1.3839	0.0000	-1.5875	0.0000	-1.7324

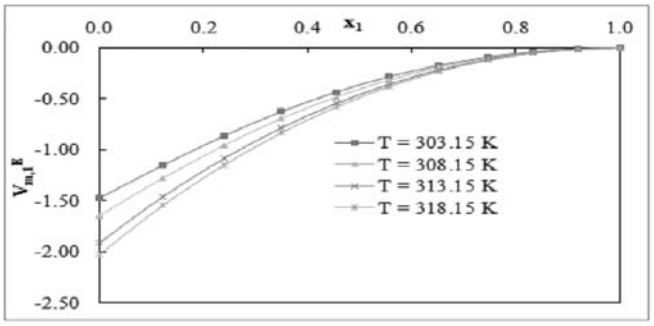

Fig. 4 Variation of $\overline{V}^{E}_{m,1}$ with mole fraction of 1, 4-BD.

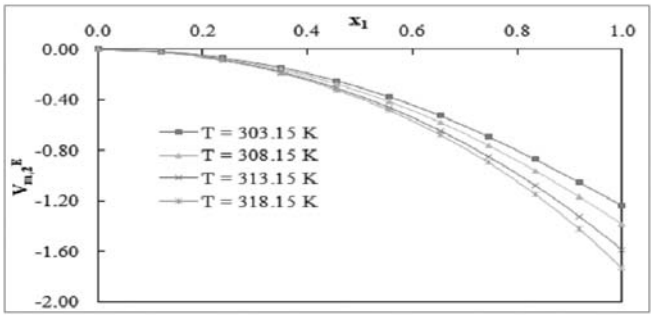

Fig. 5 Variation of $\overline{V}^{E}_{m,2}$ with mole fraction of 1, 4-BD.

By close look at Figs. 4-5 the values of $\overline{V}^{E}_{m,1}$ and $\overline{V}^{E}_{m,2}$ shows negative for the binary mixture over the whole composition range.By means, the molar volumes of each component in the binary mixture are less than their respective molar volume in the pure state, *i.e.*, there is a decrease in the volume on mixing 1, 4-BD with picolines.

In general, the negative $\overline{V}^{E}_{m,1}$, and $\overline{V}^{E}_{m,2}$ values shows the presence of significant solute-solvent interactions between unlike molecules[17] in the mixture. By close observation of negative $\overline{V}^{E}_{m,1}$, and $\overline{V}^{E}_{m,2}$ values shows that 1,4-BD-1,4-BD or picoline - picoline interactions are lesser than the 1,4-BD-picolin interactions.

Conclusion

In this paper, densities, and speeds of sound of binary mixtures of 1, 4-BD with γ-picoline along with those of pure liquids at temperatures T = (303.15 to 318.15) K at the atmospheric pressure 0.1 MPa, have been reported.Values of the excess molar volume V^{E}_{m}, excess isentropic compressibility κ^{E}_{s} and excess molar isentropic compressibility $K^{E}_{s,m}$ were obtained from experimentally measured densities and speeds of sound. Values of V^{E}_{m}, κ^{E}_{s} and $K^{E}_{s,m}$ were negative and becomes more negative with increase in temperature. The overall negative behavior of V^{E}_{m}, κ^{E}_{s} and $K^{E}_{s,m}$ may be attributed to strong ion-ion/dipole-dipole interaction and easy accommodation of picolines in the voids of 1,4-BD molecule.

References

1 **Ishihara Y., Okouchi S.** and **Uedaira H.,** Dynamics of hydration of alcohols and diols in aqueous solutions, *J. Chem. Soc., Faraday Trans.* **93** (1997) 3337-3342.

2 **Wang F., Pottel R.** and **Kaatze U.,** Dielectric properties of alkanediol water mixtures, *J. Phys. Chem.* **101** (1997) 922-929.

3 **Gerhartz W.,** Ullmann's Encyclopedia of Industrial Chemistry, 5th ed., *VCH Publishers, Deerfield Beach, FL*, **A1** (1985).

4 **Gnanakumari P.,Venkatesu P., Rama Mohan K.** and **Prabhakara Rao M.V.,** Excess volumes and excess enthalpies of N-methyl-2-pyrrolidone with branches alcohols, *Fluid Phase Equilib.* **252** (2007) 137-142.

5 **Fatemeh P., Mohammad R.Z.** and **Bahman B.,** Experimental and theoretical study on liquid-liquid equilibrium of 1-butanol+water+NH_4Cl at 298.15, 308.15 and 318.15 K, *Fluid Phase Equilib*. **325** (2012) 1-5.

6 **Blanca E.G.F., Arturo T.** and **Jacinto A.H.,** Liquid-liquid phase behavior, liquid-liquid density and interfacial tension of multicomponent systems at 298 K, *Fluid Phase Equilib.* **255** (2007) 147-159.

7 **Zhou J.G., Zhu R.J., Xu H. and Tian Y.,** Densities and excess molar volume, isothermal compressibility and isobaric expansivity of (dimethyl carbonate+n-hexane) systems at temperatures (293.15 to 313.15) K and pressures from 0.1MPa up to 40 MPa, *J. Chem. Thermodyn*. **42** (2010) 1429-1434.

8 **Zorebski E., Goralski P., Godula B.** and **Zorebski M.**, Thermodynamic and acoustic properties of binary mixtures of 1-butanol with 1,2-butanediol, *J.Chem. Thermodyn*. **68** (2014) 145-152.

9 **George J.** and **Sastry N.V.,** Densities, dynamic viscosities, speeds of sound and relative permittivities for water + alkanediols at different temperatures, *J. Chem. Eng. Data*, **48** (2003) 1529-1539.

10 **Nain A.K.,** Molecular interactions in binary mixtures of formamide with 1-butanol, 2-butanol, 1,3-butanediol and 1, 4-butanediol at different temperatures: An ultrasonic

and viscometric study, *Fluid Phase Equilib.* **265** (2008) 46-56.

11 **Yang C., Ma P.** and **Zhou Q.**, Excess molar volume, viscosity and heat capacity for the mixtures of 1, 4-butanediol + water at different temperatures, *J. Chem. Eng. Data.* **49** (2004) 582-587.

12 **Klingsberg E. (Ed.)**, Chemistry of Heterocyclic Compounds: Pyridine and its Derivatives, Interscience Publishers Inc, New York, **14**(2) (2008).

13 **Srinivasu J.V., Narendra K., Srinivasa Krishna T.** and **Subba Rao B.,** Study of volumetric and thermodynamic properties of binary mixtures 1, 4-butanediol with methylpyridine isomers at different temperatures, *J. Mol. Liq.* **216** (2016) 455-465.

14 **Pereiro A.B., Rodriguez A., Canosa J.** and **Tojo J.,** Vapor-liquid equilibria for systems of diethyl carbonate and ketones and determination of group interaction parameters for the UNIFAC and ASOG method, *Fluid Phase Equilib.* **235** (2005) 83-91.

15 **Srilakshmi M., Narendra K., Ratnakar A., Kavitha Ch.** and **Durga Bhavani M.,** Ultrasonic speed measurements in binary mixtures containing esters at temperatures from 303.15 to 318.15 K, *J. Pure Appl. Ultrason.* **38** (2016) 31-34.

16 **Iloukhani H.** and **Rostami Z.,** Densities and derived thermodynamic properties of binary mixtures of diethylcarbonate, acetophenone and 1-hexanol at T = (293.15 to 323.15) K for the liquid region and at ambient pressure, *J. Chem. Thermodyn*. **39** (2007) 1231-1240.

17 **Narendra K., Srinivasa Krishna T., Sudhamsa B., Ranjan Dey** and **Sarath Babu M.,** Thermophysical and optical studies of molecular interactions in binary mixtures of diethyl carbonate with aromatic compounds at temperatures from 298.15 to 323.15 K, *J. Chem. Thermodyn*. **103** (2016) 17-29.

J. Pure Appl. Ultrason. 39 (2017) pp. 40-42

Temperature dependent acoustical behaviour of Ir and Rh metals

Arvind Kumar Tiwari*

Department of Physics, B.S.N.V.P.G. College, Lucknow-226001, India
*E-mail: tiwariarvind1@rediffmail.com

The Coulomb and Born-Mayer potential was applied to evaluate the second and third order elastic constants of Ir and Rh metals at 273.2 K, 298.2 K and 373.2 K. The ultrasonic velocity, Debye average velocity, thermal relaxation time and acoustic coupling constant are calculated using the higher order elastic constants and other related parameters. Contribution of these parameters to the total attenuation is studied. It is found that significant contribution to the total attenuation occurs due to phonon-phonon interaction. The attenuation due to thermoelastic loss is negligible compared to phonon-phonon interaction, establishing that the major part of energy from sound wave is removed due to interaction with thermal phonons.

Keywords: Ultrasonic properties, thermoelastic relaxation, thermal conductivity, Akhieser loss.

Introduction

Extensive studies on ultrasonic attenuation in solids have been made[1-3]. The need for the characterization of materials using non-destructive evaluation has been growing steadily with the advent of newer materials and their applications under stringent conditions. Attenuation often serves as a measurement tool that leads to the formation theories to explain physical or chemical phenomena. Iridium a metal of platinum family is white, with a slight yellowish cast. It is the most corrosion-resistant metal known and was used in making the standard meter bar of Paris. Iridium has found used in making crucibles and apparatus for use at high temperature. It is also used for electrical contacts with osmium; it forms an alloy which is used for tipping pens and compass bearings. Rhodium is silvery white and at red heat slowly changes in air to the sesquioxide. Its major use is as an alloying agent. Such alloys are used for furnace windings, thermocouple elements, bushings for glass fibre production electrodes for air craft spark plugs and laboratory crucibles. Plated rhodium is used for optical instruments. It is also used for Jewellery and as a catalyst. Importance of these metals in different areas is the attraction to the author for the study of the behaviour of propagating ultrasonic wave through these metals. In the present investigation, ultrasonic attenuation due to phonon-phonon interaction and thermo elastic loss has been made in Ir and Rh metals at 273.2 K, 298.2 K and 373.2 K along <110> crystallographic direction for longitudinal and shear wave polarized along <001> and <1$\bar{1}$0> direction. The characteristic behaviour of ultrasonic propagation in the materials has been also discussed.

Theory

These metals possess face centred cubic crystal structure. The potential used for evaluation of second and third order elastic constants (SOECs and TOECs) is taken as the sum of Coulomb and Born-Mayer potentials[4]

$$\phi\ (r) = \pm\ (e^2 / r) + A\ \exp\ (-r / b)$$

where e is the electronic charge, r is nearest neighbour distance, A is the strength parameter and b is the hardness parameter.

Following Brügger's definition[5] of elastic constants and taking interaction upto second nearest neighbour distance, SOEC and TOEC are evaluated at absolute zero of temperature. Adding vibrational energy contribution to static elastic constants, one gets C_{IJ} and C_{IJK} at required temperature[6,7] as

$$C_{IJ} = C^0_{IJ} + C^{Vib}_{IJ}$$
$$C_{IJK} = C^0_{IJK} + C^{Vib}_{IJK}$$

Where superscript 0 has been used to denote SOEC and TOEC at 0K and superscript *Vib*. for temperature dependence SOEC and TOEC.

Mason theory is still widely used success-fully to study the ultrasonic attenuation at higher temperatures (~300 K) in solids. It is more reliable theory to study anharmonocity of the crystals as it involves elastic constants directly through non-linearity parameter 'D' in the evaluation of ultrasonic absorption coefficient (α).

The thermal relaxation time[8] for longitudinal is twice that of shear wave.

$$\tau_{th} = \tau_{shear} = \frac{1}{2}\tau_{long} = \frac{3K}{C_V \bar{V}^2}$$

K is thermal conductivity, C_V is specific heat per unit volume, $\bar{V}$ is the Debye average velocity of the ultrasonic wave and given as

$$3/\bar{V}^3 = 1/V_l^3 + 2/V_s^3$$

Thermoelastic loss[8] is obtained by

$$(\alpha / f^2)_{th} = \frac{4\pi^2 < \gamma_i^j >^2 KT}{2\rho V_{long}^5}$$

$< \gamma_i^j >$ is the average Grüneisen numbers; j is the direction of propagation and i is the mode of propagation ρ is density of the material and T is the temperature in the Kelvin scale.

The ultrasonic absorption coefficient over frequency square $(\alpha/f^2)_{\text{Akh}}$ is given by $(\omega\tau<<1)$[8]

$$(\alpha / f^2)_{Akh.} = \frac{4\pi^2 \tau\, E_o (D/3)}{2\rho V^3}$$

To evaluate $(\alpha/f^2)_{\text{Akh}}$ one has to evaluate anharmonic parameter 'D' which is the measure of the conversion of acoustic energy into thermal energy and is obtained by

$$D = 9 < (\gamma_i^j)^2 > - \frac{3 < \gamma_i^j >^2 C_V T}{E_o}$$

By determining D_{long} and D_{Shear} for longitudinal and shear wave; $(\alpha/f^2)_{\text{Akh.long.}}$ and $(\alpha/f^2)_{\text{Akh.shear}}$ can be evaluated.

Results and Discussion

The ultrasonic attenuation caused by electron-phonon interaction, phonon-phonon interaction and thermoelastic relaxation is evaluated using nearest neighbour distance r_0=1.919Å, 1.902Å and hardness parameter b=0.313Å, 0.311Å for Ir and Rh metals respectively at different temperatures. The SOEC and TOEC have been evaluated at different temperatures and are presented in Table 1. The experimental values of second and third order elastic constants of other metals of the group are available[9]. There is good agreement between the present values and the reported experimental values. The six third order elastic constants are very important to study the anhormonocity of the metals and reveal the various inherent properties of the metals. We have calculated Grüneisen parameters along <110> direction for longitudinal wave over 39 modes and for shear wave polarized along <001> direction over 14 modes and polarized along <1$\bar{1}$0> direction over 20 modes. The values of Grüneisen parameters along with non-linearity coupling constants (D_l and D_s) are presented in Table 2. These metals have the same trend of variation with temperature for D_l and D_s like other heavy rare-earth metals[10].

It is obvious from Tables 3 that values of the thermo-elastic loss $(\alpha/f^2)_{\text{th}}$ is negligible in comparison to Akhieser type attenuation $(\alpha/f)_{\text{Akh}}$. This is because of the low values of thermal conductivity and higher values of Debye average velocities of the waves. A greater value of longitudinal wave in comparison to shear wave is due to greater value of non-linearity parameter D_l in comparison to D_s. It can be seen from the Table 3 that Ultrasonic attenuation (both for Akhieser and thermo-elastic loss) increases with increase in temperature and

Table 1 – Second and third order elastic constants (SOEC and TOEC) of Ir and Rh at temperatures 273.2 K, 298.2 K and 373.2 K [× 10^{11} Dyne/cm^2].

	Temp. (K)	C_{11}	C_{12}	C_{44}	C_{111}	C_{112}	C_{123}	C_{144}	C_{166}	C_{456}
Ir	273.2	7.339	7.844	8.174	-91.7	-31.7	10.7	11.7	-32.6	11.5
	298.2	7.398	7.821	8.181	-91.9	-31.7	10.6	11.7	-32.6	11.5
	373.2	7.576	7.753	8.202	-92.5	-31.5	10.4	11.8	-32.7	11.5
Rh	273.2	7.294	8.162	8.494	-90.6	-32.9	11.1	12.1	-33.8	11.9
	298.2	7.352	8.139	8.501	-90.8	-32.9	11.0	12.1	-33.8	11.9
	373.2	7.528	8.069	8.523	-91.4	-32.8	10.8	12.2	-33.9	11.9

Table 2 – Average Grüneisen numbers $< \gamma_i^j >_l$ for longitudinal wave, square average Grüneisen numbers $<(\gamma_i^j)^2>_l$ for longitudinal wave, square average Grüneisen numbers $<(\gamma_i^j)^2>_{s1}$ for shear wave polarised along <001> direction, square average Grüneisen numbers $<(\gamma_i^j)^2>_{s2}$ for shear wave polarised along $<1\bar{1}0>$ direction, non-linearity parameters D_l for longitudinal wave, D_{s1} for shear wave polarised along <001> direction and D_{s2} for shear wave polarised along $<1\bar{1}0>$ direction [all along <110> direction].

Metals	Temp. (K)	$< \gamma_i^j >_l$	$<(\gamma_i^j)^2>_l$	$<(\gamma_i^j)^2>_{s1}$	$<(\gamma_i^j)^2>_{s2}$	D_l	D_{s1}	D_{s2}
Ir	273.2	3.084	202.60	10.098	7.454	1775.7	90.882	67.082
	298.2	3.770	287.44	14.052	9.904	2518.74	126.45	89.132
	373.2	9.040	1441.4	67.235	42.543	12611.9	605.07	382.86
Rh	273.2	1.614	72.695	4.203	4.253	640.597	37.818	38.268
	298.2	1.839	88.693	5.016	4.875	781.087	45.135	43.875
	373.2	2.848	181.20	9.659	8.412	1593.7	86.922	75.699

Table 3 – Ultrasonic attenuation $(\alpha/f^2)_{th}$, $(\alpha/f^2)_{Akh.long}$ and $(\alpha/f^2)^*_{Akh.shear}$ and $(\alpha/f^2)\#_{Akh.shear}$ along <110> crystallographic direction [in 10^{-17} Nps^2/cm].

Metals	Temp. (K)	$(\alpha/f^2)_{th}$	$(\alpha/f^2)_{Akh.long}$	$(\alpha/f^2)^*_{Akh.shear}$	$(\alpha/f^2)\#_{Akh.shear}$
Ir	273.2	16.168	3453.667	75.055	55.399
	298.2	25.409	5399.099	116.371	82.021
	373.2	167.275	34059.160	724.421	472.343
Rh	273.2	1.882	492.594	11.569	11.707
	298.2	2.571	656.354	15.248	14.823
	373.2	7.039	1715.95	38.880	33.860

* and # polarized along <001> and $<1\bar{1}0>$ directions respectively.

maximum at 373.2 K for both the metals. The same order of the values are found in previously investigated other rare-earth Ce, Yb and Th metals[10].

Conclusion

Thus it is established that our theoretical approach for the calculation of second and third order elastic constants and ultrasonic attenuation at different temperatures is still valid for Ir and Rh metals. The behaviour of ultrasonic absorption coefficients and other related parameter like non-linearity parameters at different temperatures can be used for the characterization of the materials because it is well connected to elastic and thermal properties of the metals. The results may be directly applicable to the material producing industries for the characterization of the materials during the process control.

References

1 **Tripathy C., Singh D.** and **Paikaray R.,** Elastic and ultrasonic properties of LaPn (Pn=N, P, As, Sb, Bi), *J. Pure Appl. Ultrason.* **38** (2016) 99-102.

2 **Kumar J., Shrivastava S.K.** and **Kailash**, Ultrasonic wave propagation through calcium oxide single crystal in high temperature range, *J. Pure Appl. Ultrason.*, **38** (2016) 110-114.

3 **Jaykumar T.** and **Kumar A.,** Characterization of metallic materials through elastic properties, *J. Pure Appl. Ultrason.*, **36** (2014) 29-35.

4 **Born M.** And **Mayer J.E.**, Zur Gitterthorie der Ionenkristalle, *Z. Phys.*, **75** (1931) 1-18.

5 **Brugger K.,** Thermodynamic definition of higher order elastic coefficients, *Phy. Rev.*, **133** (1964) A1611-A1612.

6 **Mori S.** and **Hiki Y.,** Calculation of third and fourth order elastic constants of alkali halide crystals, *J. Phys. Soc. Jpn.*, **45** (1975) 1449-1456.

7 **Ghate P.B.,** Third order elastic constants of alkali halide crystals, *Phys. Rev.*, **139** (1965) A 1666-A1674.

8 **Mason W.P.,** Physical Acoustics, Academic Press, New York, IIIB (1965) p. 237.

9 **Gupta A.K., Gupta A., Tripathi S., Bhalla V.** and **Singh D.,** Ultrasonic properties of hexagonal closed packed metals, *Universal J. Mat. Sc.*, **1** (2013) 63-68.

10 **Yadav R.R., Singh D.** and **Tiwari A.K.,** Ultrasonic evaluations in rare-earth metals, *J. Acoust. Soc. Ind.*, **30** (2002) 59-63.

J. Pure Appl. Ultrason. 39 (2017) pp. 43-48

Mechanical and thermophysical properties of lutetium monochalcogenides: an ultrasonic study

Amit Kumar[1,*], Devraj Singh[2], Ram Krishna Thakur[1] and Raj Kumar[3]

[1]Amity School of Applied Sciences, Amity University Haryana, Manesar-122413, India
[2]Department of Applied Physics, Amity School of Engineering & Technology, Bijwasan, New Delhi-110061, India
[3]Department of Physics, Gurgaon Institute of Technology & Management, Gurgaon-122413, India
*E-mail: amitrana1711@gmail.com

The paper presents theoretical temperature dependent mechanical and thermophysical properties of lutetium monochalcogenides using ultrasonic analysis. The higher order elastic constants are evaluated using Coulomb and Born-Mayer potential upto second nearest neighbour. The second order elastic constants are used to compute mechanical parameters such as bulk modulus, shear modulus, tetragonal modulus, Poisson's ratio, Zener anisotropy factor and fracture to toughness ratio for finding future performance of the chosen materials at room temperature. The second order elastic constants are further applied to find out the ultrasonic velocities <100>, <110> and <111> crystallographic directions in the temperature range 100-300 K. Finally Debye temperature, ultrasonic Grüneisen parameters and first order pressure derivatives of lutetium monochalcogenides are computed using the second and third order elastic constants. The obtained results are discussed in correlation with available results on these properties for the chosen materials.

Keywords: Lutetium monochalcogenides, elastic properties, ultrasonic properties.

Introduction

The materials characterization by ultrasonics plays very important role for materials' scientists and engineers since a long period[1-2]. The rare-earth monochalcogenides and monopnictides are uniformly valuable for materials devices especially for the advancement in the area of electronics and spintronics[3-4]. Several investigators have investigated the physical properties of rare-earth monochalcogenides and monopnictides[5-8]. Seddik *et al.*[5] investigated the pressure induced structural phase transformation and mechanical properties of lutetium monochalcogenides. LuX (X:S, Se, Te) were studied by means of the full-potential augmented plane wave plus local orbitals method. Mir *et al.*[6] applied density functional theory (DFT) within the framework of generalized gradient approximation to investigate the structural, elastic, mechanical, and phonon properties of lutetium monopnictides. The electronic structure calculations were performed for the rare-earth (RE) nitrides using DFT calculations within the LSDA+U approach (local spin density approximation with Hubbard-U corrections) by Larson *et al.*[7]. With use of synchrotron radiation, the powder X-ray diffraction of rare-earth lanthanide monoarsenides LnAs (Ln = Pr, Nd, Sm, Gd, Dy and Ho) with a NaCl-type structure has been studied up to 60 GPa at room temperature by Shirotani *et al.*[8].

Overall, we found only few studies on lutetium monochalcogenides. This motivates us to study elastic and ultrasonic properties of LuX. In present investigation, first we computed second and third order elastic constants (SOECs and TOECs) with the application of Coulomb and Born-Mayer potential using lattice and hardness parameters in the temperature range 100-300K. The evaluated values of SOECs are applied to compute mechanical properties of these materials such as bulk modulus, shear modulus, tetragonal modulus, Poisson's ratio, Zener anisotropy factor and fracture to toughness ratio for finding materials' future performance at room temperature. Further, SOECs and TOECs are used to find

temperature dependent ultrasonic velocities, ultrasonic Grüneisen parameters, Debye temperature and first order pressure derivatives along <100>, <110> and <111> crystallographic directions. The results are discussed with available similar type of materials.

Theory

Coulomb and Born -Mayer potential[9] has been used to evaluate SOECs and TOECs of LuX (X: S, Se, Te). The interionic potential is the summation of Coulomb and Born -Mayer potentials.

$$\phi(R) = \phi(C) + \phi(B) \tag{1}$$

Where $\phi(B)$ is the Born- Mayer potential and $\phi(C)$ is the Coulomb potential and are given by

$$\phi(B) = A\ \exp.\left(\frac{-r}{b}\right) \text{ and } \phi(C) = \pm\frac{e^2}{r} \tag{2}$$

Where r is the nearest neighbour distance, e is the electronic charge, b is the hardness parameter and A is the strength parameter given by

$$A = -3b\frac{e^2}{r_0}S_3^{(1)}\frac{1}{6\exp(-\rho_0)+12\sqrt{2}\exp(-\sqrt{2}\rho_0)} \tag{3}$$

The Burgger's definition[10] has been applied to find SOECs and TOECs. From lattice dynamics we can say lattice energy transforms with temperature[11]. Hence SOECs and TOECs at a particular temperature can be obtained on the addition of vibrational energy contribution and the static elastic constants.

$$\begin{aligned} C_{IJ} &= C_{IJ}^0 + C_{IJ}^{Vib} \\ C_{IJK} &= C_{IJK}^0 + C_{IJK}^{Vib} \end{aligned} \tag{4}$$

0 (zero) and *Vib* represent the static and vibrational contribution of elastic constants. The detail expressions for C_{IJ} and C_{IJK} are given elsewhere[12].

SOECs and TOECs are used to compute the mechanical constants like bulk moduli *(B)*, shear or rigidity moduli *(G)*, tetragonal moduli (C_s), Zener anisotropy factor (A), toughness to fracture ratio *(G/B)* and Poisson's ratio (σ). Formulae to find these mechanical constants are given in literature[6]. The strength, stability and hardness of the materials are determined from these parameters. The stability of a cubic crystal given by Born[6] and is presented in terms of elastic constants as follows.

$$B = \frac{C_{11}+2C_{12}}{3} > 0,\ Cs = \frac{C_{11}-C_{12}}{2} > 0,\ C_{44} > 0, \tag{5}$$

Ultrasonic velocity is important parameter for the characterization of materials. The velocity of propagation of ultrasonic wave through the anisotropic solids along <100>, <110>, <111> directions will depends on the orientation of strains along the respective directions. Accordingly we are having three types of velocities: one longitudinal V_L and two shear velocities V_{S1}, V_{S2}. When ultrasonic wave passes through a medium, then there are three modes of propagation, one longitudinal acoustical and two transverse acoustical. Hence we obtained three types of velocities one longitudinal (V_L) and two shears (V_{S1}, V_{S2}). The expressions of ultrasonic velocities for longitudinal and shear waves velocities (V_L and V_S) are found elsewhere[12].

The Debye average velocity V_D has been obtained from Debye theory[13] is given by average of the longitudinal and shear velocities is given by the following expression.

$$V_D = \left[\frac{1}{3}\left\{\frac{1}{V_L^3}+\frac{2}{V_s^3}\right\}\right]^{-\frac{1}{3}}; \text{Along <100> and <111> direction} \tag{6}$$

$$V_D = \left[\frac{1}{3}\left\{\frac{1}{V_L^3}+\frac{1}{V_{s1}^3}+\frac{1}{V_{s2}^3}\right\}\right]^{-\frac{1}{3}}; \text{Along <110> direction} \tag{7}$$

From Debye average velocity V_D is applied to compute Debye temperature (θ_D)[13] can be calculated with Eq. (8).

$$\theta_D = \frac{h}{k_B}\left(\frac{3n}{4\pi}\frac{N\rho}{M}\right)^{\frac{1}{3}}V_D \tag{8}$$

Where k_B is Boltzmann constant, N is Avogadro's number, h is Planck's constant, ρ is the density, M is molecular weight and n is the number of atoms in the molecule.

The Grüneisen parameters describe the phonon contribution to number of anharmonic characteristic of solids such as specific heat of lattice, thermal expansion and thermal conductivity. These parameters show as diverse weighted averages of Grüneisen tensor of first order. For anisotropic elastic continuum, the components of Grüneisen tensor in terms of SOECs and TOECs have been derived by Brugger[14]. Formulae for Grüneisen parameters along different crystallographic directions are specified in literature[13].

One of the important features[15] of the present investigation is the calculation of first order pressure derivatives of elastic constants at different temperatures. The expressions for first order pressure derivatives *(dCij/dp)* are given below:

$$\frac{dC_{11}}{dp} = \frac{-1}{C_{11}+2C_{12}}(2C_{11}+2C_{12}+C_{111}+2C_{112}) \quad (9)$$

$$\frac{dC_{12}}{dp} = \frac{-1}{C_{11}+2C_{12}}(-C_{11}-C_{12}+2C_{112}+C_{123}) \quad (10)$$

$$\frac{dC_{11}}{dp} = \frac{-1}{C_{11}+2C_{12}}(C_{11}+2C_{12}+C_{144}+2C_{456}) \quad (11)$$

Results and Discussion

Elastic properties of a solid are essential because the elastic constants of solids provide a link between the mechanical and dynamical behavior of crystals and give necessary information concerning the nature of the forces performing in solids. The SOECs and TOECs have been computed by using two basic parameters *i.e.*, nearest neighbour distance *(r_0)* and hardness parameter *(b)*. These input parameters are given in Table 1 with the density ρ of LuX.

The computed results of temperature dependent SOECs and TOECs are given in Table 2.

Table 1 – r_0, b and density (ρ) of the LuX.

Material	r_0 (in Å)	b (in Å)	ρ (in g/cc)
LuS	2.67	0.29	8.95
LuSe	2.78	0.29	8.023
LuTe	2.97	0.29	7.149

It is clear from the Table 2 that, out of nine elastic constants, four (*i.e.*, C_{11}, C_{44}, C_{112} and C_{144}) are increasing and other four (*i.e.*, C_{12}, C_{111}, C_{166} and C_{123}) are decreasing with the temperature while C_{456} is found to be unaffected. The increase or decrease in stiffness constants is due increase or decrease in atomic interaction with temperature. This type of behaviour has been found already in other NaCl-type materials like lanthanum[16] and cerium[12] monochalcogenides. We compare our results with the results of Seddik *et al.*[5] as shown in Table 2. Our computed results of SOECs are less, much or approximate equal with results of Seddik *et al.*[5]. They used density functional theory and considered interaction of atoms upto many nearest neighbourhood, while we considered upto second nearest meighbour.

The obtained results of SOECs and TOECs are applied to compute the bulk modulus *(B)*, shear modulus *(G)*, tetragonal moduli *(C_S)*, Poisson's ratio (σ), Zener anisotropy factor *(A)* and ratio *B/G*. These values are given in Table 3 at room temperature..

Table 3 shows *B/G* ratio is less than 1.75, which indicates that LuX have brittle nature. LuX fulfilled the Born criterion[6] so we can say that these materials are mechanically stable. Anisotropy factor is less than one for these materials so these materials have anisotropic behavior. The mechanical properties of LuS are better than the other chosen materials LuSe and LuTe.

The ultrasonic velocity is key parameter of the materials to provide information about the crystallographic texture. The ultrasonic velocities (V_L and V_S) can be obtained by SOECs and values density of the materials for longitudinal and shear modes of propagation along <100>, <110> and <111> directions. Further these ultrasonic velocities are applied to find out

Table 2 – Temperature dependent SOECs and TOECs of LuX [in the unit GPa]

Material	Temp. (K)	C_{11}	C_{12}	C_{44}	C_{111}	C_{112}	C_{123}	C_{144}	C_{166}	C_{456}
LuS	100	60.3	17.6	18.5	-954	-72.3	25.5	30.6	-75.9	30.4
	200	62.0	16.7	18.6	-961	-69.1	20.6	30.9	-76.2	30.4
	300	63.9	15.8	18.7	-970	-65.9	15.6	31.1	-76.5	30.4
	300	280.7[5]	21.8[5]	147.8[5]						
LuSe	100	55.9	14.6	15.5	-905	-59.9	20.9	26.1	-63.5	25.9
	200	57.6	13.8	15.6	-915	-56.6	15.9	26.3	-63.7	25.9
	300	59.5	12.9	15.7	-922	-53.4	10.8	26.5	-64.0	25.9
	300	235.3[5]	16.3[5]	109.2[5]						
LuTe	100	48.9	10.8	11.6	-823	-43.6	14.7	20.1	-47.1	19.9
	200	50.6	10.0	11.7	-831	-40.3	9.6	20.2	-47.3	19.9
	300	52.4	9.2	11.7	-841	-37.0	4.7	20.3	-47.5	19.9
	300	189.3[5]	8.9[5]	95.9[5]						

Table 3 – B, G, C_S, σ, A and B/G of LuX at 300K.

Material	B (in GPa)	G (in GPa)	Cs (in GPa)	σ	A	B/G
LuS	3.18	2.23	2.41	0.60	0.78	1.43
LuSe	2.84	2.08	2.33	0.53	0.67	1.37
LuTe	2.36	1.83	2.16	0.45	0.54	1.29

Table 4 – The ultrasonic velocities (in km/s) of LuX.

Material	Direction	Velocity	100 K	200 K	300 K
LuS	<100>	V_L	2.59	2.63	2.67
		$*V_{S1}=V_{S2}$	1.44	1.44	1.44
		V_D	1.88	1.89	1.90
	<110>	V_L	2.53	2.54	2.55
		$\$V_{S1}$	1.44	1.44	1.44
		$\#V_{S2}$	2.18	2.24	2.31
		V_D	1.82	1.84	1.85
	<111>	V_L	2.51	2.51	2.52
		$@V_{S1}=V_{S2}$	1.51	1.54	1.57
		V_D	1.93	1.96	1.99
LuSe	<100>	V_L	2.64	2.68	2.72
		$*V_{S1}=V_{S2}$	1.39	1.39	1.39
		V_D	1.84	1.85	1.86
	<110>	V_L	2.51	2.53	2.54
		$\$V_{S1}$	1.39	1.39	1.39
		$\#V_{S2}$	2.26	2.33	2.40
		V_D	1.79	1.80	1.82
	<111>	V_L	2.47	2.47	2.48
		$@V_{S1}=V_{S2}$	1.53	1.57	1.60
		V_D	1.94	1.97	2.00
LuTe	<100>	V_L	2.61	2.66	2.70
		$*V_{S1}=V_{S2}$	1.27	1.28	1.28
		V_D	1.71	1.72	1.73
	<110>	V_L	2.41	2.42	2.44
		$\$V_{S1}$	1.27	1.28	1.28
		$\#V_{S2}$	2.30	2.38	2.45
		V_D	1.68	1.69	1.70
	<111>	V_L	2.33	2.34	2.34
		$@V_{S1}=V_{S2}$	1.52	1.56	1.60
		V_D	1.89	1.92	1.95

*, $, # and @ polarized along <100>, <001>, <1$\bar{1}$0> and <$\bar{1}$10> directions respectively.

the Debye average velocity (V_D) using Eqs. (6)-(7) and are shown in Table 4.

The ultrasonic velocity increases with the increase of temperature in all directions. It is obvious from Table 4 that the Debye average velocity is highest along <111> direction for all the materials. So <111> will be most appropriate for wave propagation for the chosen material LuX. This type of behaviour of wave velocity for the chosen material is similar to rare-earth monochalcogenides of lanthanum[16] and cerium[12].

Table 5 – Direction dependent Debye temperature and Grüneisen parameters of LuX at room temperature

Material	Direction	θ_D(K)	$<\gamma_i^j>_1$	$<(\gamma_i^j)^2>_1$	$<(\gamma_i^j)^2>_{s1}$	$<(\gamma_i^j)^2>_{s2}$
LuS	<100>	212	0.42	1.65	0.11	0.11
	<110>	206	-0.71	2.07	0.11	2.86
	<111>	222	-0.63	1.84	1.95	1.95
LuSe	<100>	199	0.42	1.73	0.11	0.11
	<110>	195	-0.70	2.14	0.10	3.04
	<111>	174	-0.64	1.88	2.07	2.07
LuTe	<100>	170	0.41	1.87	0.11	0.11
	<110>	212	-0.69	2.31	0.09	5.37
	<111>	196	-0.65	1.96	2.29	2.29

The Debye temperature is an important parameter, which is division line of classical and quantum behavior of the material and is obtained with Eq. (8) using Debye model. The Grüneisen parameter is function of SOECs and TOECs. These parameters have a number of modes of propagation along different directions, so we used average parameter. These parameters with Debye temperature are presented in Table 5 at room temperature (≈300K).

It is observed from Table 5 that Debye temperature is highest *i.e.,* 222K along <111> direction for LuS and lowest 170 K along <100> direction for LuTe. So we can say that LuS material will be more suitable at higher temperature. The trend is comparable with praseodymium monopnictides[17].

An analysis on pressure derivatives of elastic constants gives useful information on the inter-atomic forces, inter-ionic potentials and on anharmonic properties of crystalline solids[17]. The first order pressure derivatives (FOPDs) of LuX are the function of SOECs and TOECs and have been computed with Eqs. (9)-(11). Temperature dependent FOPDs LuX are visualized in Figs. 1-3.

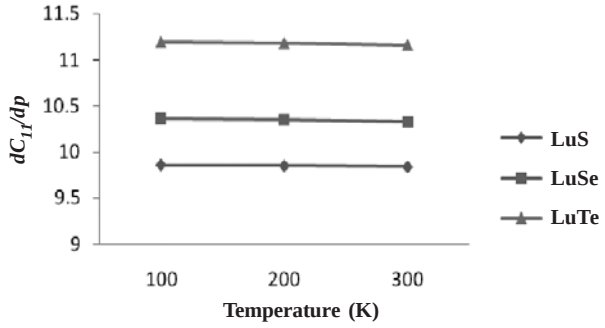

Fig. 1 FOPDs *(dC_{11}/dp)* vs. temperature of LuX

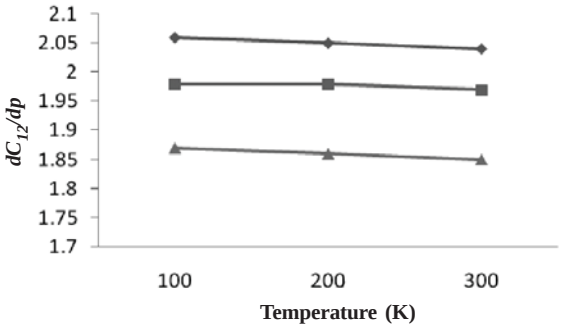

Fig. 2 FOPDs *(dC_{12}/dp)* vs. temperature of LuX

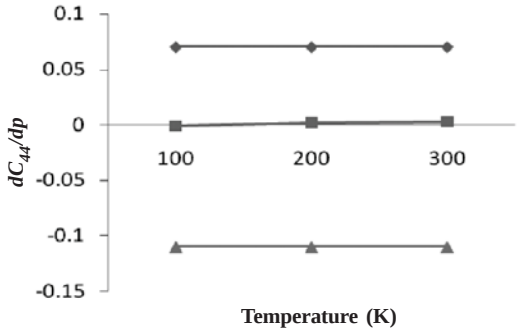

Fig. 3 FOPDs *(dC_{44}/dp)* vs. temperature of LuX

The pressure-induced variations to the elastic constants (*i.e., dC_{11}/dp*) are relatively large compared with dC_{12}/dp and dC_{44}/dp. This pattern of elasticity-pressure dependence will be reproduced in the corresponding variations of wave velocities with pressure, which in turn influence the SOECs as is observed in the ultrasonic measurements by Verlinden *et al.*[18] and Nagasawa *et al.*[19]. The FOPDs increase with temperature as observed by Kumar *et al.*[20].

Conclusion

In this endeavor, the Coulomb and Born-Mayer potential has been applied to compute the second and third order elastic constants of LuX. We have also calculated the mechanical constants such as bulk moduli, shear moduli, tetragonal moduli, Zeners' anisotropic ratio, fracture to toughness ratio (B/G) and Poisson's ratio for these materials successfully for the materials' stability and strength. The investigation verifies that the materials are mechanically stable and possess anisotropy on elasticity and brittle nature. The mechanical properties of LuS are dominant over LuSe and LuTe. The Debye average ultrasonic velocities seems to be better along <111> crystallographic direction. The thermal properties such as Debye temperature and ultrasonic Grüneisen parameter also expose that these materials have better performance at room temperature due to their more or less metallic character of LuX. The FOPDs increase with temperature. The achieved results of present investigation on rare-earth materials LuS, LuSe and LuTe are valuable for the futuristic applications of these materials as well as for further research.

References

1 **Nampoothiri J., Sri Harini R., Nayak S.K., Raj B.** and **Ravi K.R.,** Post in-situ reaction ultrasonic treatment for generation of $Ale_{4.4}Cu/TiB_2$ nanocomposite: A route to enhance the strength of metal matrix nanocomposites, *J. Alloys Compd.,* **683** (2016) 370-378.

2 **Wan M., Yadav R.R., Singh D., Panday M.S.** and **Rajendran V.,** Temperature dependent ultrasonic and thermo-physical properties of polyaniline nanofibers reinforced epoxy composites, *Composites Part B* **87** (2016) 40-46.

3 **Vaitheeswaran G., Petit L., Svane A., Kanchana V.** and **Rajagopalan M.,** Electronic structure of praseodymium monopnictides and monochalcogenides under pressure, *J. Phys.: Condens. Matter,* **16** (2004) 4429-4440.

4 **Coban C., Colakoglu K.** and **Ciftci Y.O.,** First principles predictions on mechanical and physical properties of HoX (X = As, P), *Mat. Chem. Phys.,* **125** (2011) 887-894.

5 **Seddik T., Semari F., Khenata R., Bouhemadou A.** and **Amrani B.,** High pressure phase transition and elastic properties of lutetium chalcogenide, *Physica B* **405** (2010) 394-399.

6 **Mir S.H., Jha P.C., Islam M.S., Banarjee A., Luo W., Dabhi S.D., Jha P.K.** and **Ahuja R.,** Static and dynamical properties of heavy actinide monopnictides of lutetium, *Sci. Rep.* **6** (2016) 29309.

7 **Larson P., Lambrecht W.R.L., Chantis A.** and **Van Schilfgaarde M.,** Electronic structure of rare-earth nitrides using the LSDA+U approach: importance of allowing 4f orbitals to break the cubic crystal symmetry, *Phys. Rev. B* **75** (2007) 045114.

8 **Shirotani I., Yamanashi K., Hayashi J., Tanaka Y., Ishimatsu N., Shimomura O.** and **Kikegawa T.,** Phase transitions of LnAs (Ln = Pr, Nd, Sm, Gd, Dy and Ho) with NaCl-type structure at high pressures, *J. Phys.: Condens. Matter* **13** (2001) 1939.

9 **Born M.** and **Mayer J.E.,** Zür Gittertheorie der Ionenkristalle, *Z. Phys.* **75** (1931) 1-18.

10 **Brugger K.,** Thermodynamic definition of higher order elastic coefficients. *Phys. Rev.* **133** (1964) A1611-A1612.

11 **Liebfried G.** and **Haln H.,** Zur temperaturabhangigkeit der elastischen konstantaaen von alkali halogenidid kristallen, *Z. Phys.* **150** (1958) 497-525.

12 **Bhalla V., Singh D.** and **Jain S.K.,** Mechanical and thermophysical properties of cerium monopnictides, *Int. J. Thermophys.* **37** (2016) 33.

13 **Mason W.P.** *Physical Acoustics*. Academic Press, New York, **IIIB** (1965).

14 **Brugger K.,** Generalized Grüneisen parameters in anisotropic Debye model, *Phys. Rev.,* **137** (1965) A1826-A1827.

15 **Lubarda V.A.,** Apparent elastic constants of cubic crystals and their pressure derivatives, *Int. J. Non-Linear Mech.* **34** (1999) 5-11.

16 **Yadav R.R.** and **Singh D.,** Ultrasonic attenuation in lanthanum monochalcogenides, *J. Phys. Soc. Jpn.,* **70** (2001) 1825-1832

17 **Bhalla V., Kumar R., Tripathy C.** and **Singh D.,** Mechanical and thermal properties of praseodymium monopnictides: an ultrasonic study, *Int. J. Mod. Phys. B* **27**, 1350116

18 **Verlinden A., Suzuki T., Delaey L.** and **Guenin G.,** Third order elastic constant of B-Cu-Zn-Al as a function of the temperature, *Script. Met.* **18** (1984) 975.

19 **Nagasawa A., Makita T.** and **Takagi Y.,** Anharmonicity and martensitic phase transition in β-phase alloys, *J. Phys. Soc. Jpn.* **51**(1982) 3876.

20 **Kumar J., Kailash, Kumar V.** and **Chaudhary A.K.,** Temperature dependence of pressure derivatives of higher order elastic constants of TeO crystal, *Asian J. Chem.* **23** (2011) 5601-5604.

J. Pure Appl. Ultrason. 39 (2017) pp. 49-54

Study of frequency and concentration dependence of ultrasonic attenuation of NiO nanoparticle embedded in polyvinilidyne fluoride

Chayan K. Karmakar, Biplab Dutta and Sampad Mukherjee*

Department of Physics, Indian Institute of Engineering Science and Technology, Shibpur, Howrah-711103, India
*E-mail: smukherjee.besu@gmail.com

In this work the frequency dependent attenuation coefficient of NiO embedded polyvinilidyne fluoride (PVDF) for different concentrations has been studied by the ultrasonic transmission technique. The NiO nanoparticles have been prepared by hydrothermal route and the sample was stirred with PVDF solution (by using DMF as solvent) and the thin film was prepared by slow evaporation method. The sample having different concentrations as well as neat PVDF film were taken for ultrasonic study. Then the amplitude versus time data has been collected from the ultrasonic pulsar/receiver instrument USLT 2000 by A-scan process. The readings are taken by using the transducer of central frequency 500 kHz. To convert this data in time-domain to frequency- domain, Fast Fourier transformation (FFT) has been done. From the result, the ultrasonic absorption increases with the increase of concentration of the sample for a given frequency and this is obvious as the number density of the scatterer increases. Ultrasonic absorption increases with the increase of frequency for a given concentration of the sample as the scattering increases in the Rayleigh region ($\lambda >>$ a, the particle size).

Keywords: Nanoparticle, ultrasonic absorption, FFT.

Introduction

The polymer PVDF[1-7] having structure[$(-CH_2-CF_2)_n$], shows piezoelectric, pyroelectric and ferro-electric properties[7-11]. This polymer has five different crystalline phases like α, β, γ, δ and ε[6]. Among them β phases is most important due to its better piezoelectric, ferroelectric and pyroelectric property. The electroactive β-phase[2, 5] fraction in PVDF matrix has been achieved including NiO in different concentration. In this work the nucleation of electroactive β phase in PVDF in addition of NiO as well as the structural, optical and sound absorption properties of the nanocomposite films have been studied.. Attenuation of ultrasonic wave[12-16] occurs mainly due to scattering and absorption by the constituents of the medium. Detailed analysis of the structural, sound attenuation properties of the NONP (NiO nanoparticle) loaded PVDF films have been given in this study.

Experimental

Synthesis of nickel oxide loaded PVDF nanocomposite films

The nickel oxide nanoparticles were synthesized by modified hydrothermal method at 200°C. The nickel oxide nanoparticles loaded PVDF films were synthesized by the simple solution casting method. In this typical synthesis procedure, 500 mg of PVDF was dissolved in 20 ml DMF under vigorous stirring at 60°C and the complete dissolution of PVDF in DMF was achieved. Then a certain weight percent (0.25, 0.5, 0.75 & 1 wt%) of the as synthesized nickel oxide nanoparticles were added to the solution of PVDF and vigorously stirred for 16 hours followed by a 30 min sonication to obtain a homogeneous mixture. The nanocomposite films were prepared by casting the mixture in a Petri dish, and the solvent was evaporated at 90°C. The samples of different weight percentage are shown in the Table 1.

Table 1

Weight Percent	Sample
0 (Neat)	S_0
0.25	S_1
0.5	S_2
0.75	S_3
1.00	S_4

Results and Discussion

X-ray diffraction analysis (XRD)

Figure 1 shows the X-ray diffraction (XRD) pattern of synthesized nickel oxide nanoparticles and the comparison between XRD pattern of the neat PVDF (S_0) and PVDF with nickel oxide nanoparticles (S_1, S_2 as mentioned in Table 1) are as shown in the Fig. 2. XRD pattern of nickel oxide nanoparticles reveal well crystalline nature of the sample. In this pattern the diffraction peaks at 2θ values 37.04°, 43.16°,62.71°, 75.19°, 79.3° correspond to the (101), (012), (110), (113) and (006) planes of the crystalline phase of rhombohedral nickel oxide (NiO) according to the JCPDS no. 44-1159 (a = 2.9521 Å, b =7.2275 Å). XRD pattern of the neat PVDF (S_0) and PVDF nanocomposite films shows the peaks positioned at 2θ = 17.5º (100), 18.2º(020), 19.8º (021), and 26.6º ((201), (310)) of the neat PVDF can be assigned to the nonpolar α phase of PVDF. Peaks at 2θ values 37.04° (101) and 43.16° (012) can be assigned to

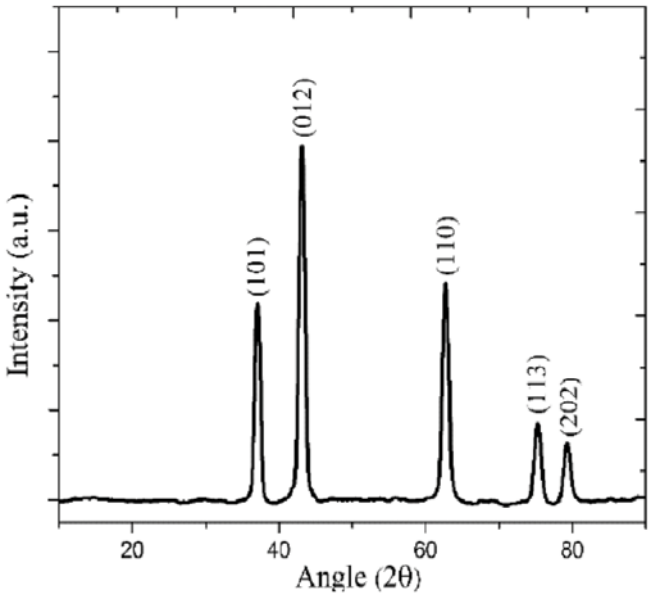

Fig. 1 X-ray diffraction (XRD) pattern of synthesized nickel oxide nanoparticles.

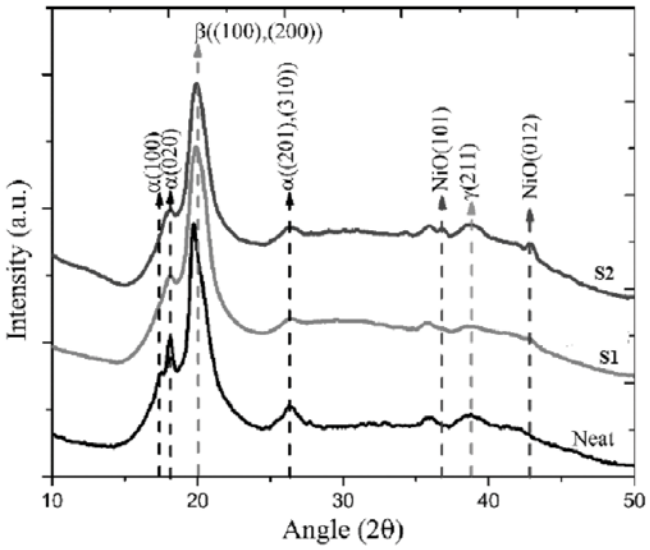

Fig. 2 Comparison between XRD pattern of the neat PVDF and PVDF with nickel oxide nanoparticles (S_1, S_2).

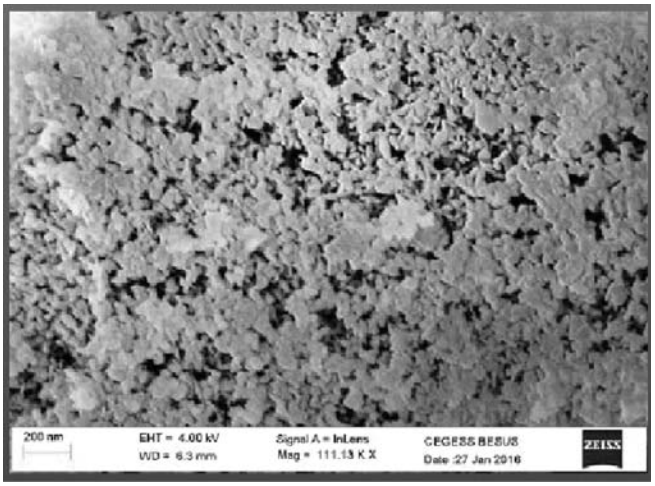

Fig. 3 FESEM image of the NiO nanoparticles.

the crystalline NiO nanoparticles which infer the successful incorporation of NONPs in PVDF matrix. This pattern also shows that the peaks corresponding to the α phase of PVDF (positioned at 17.5º, 18.2º, 19.8º and 26.6º) decrease with the increase of loading fraction of nanoparticles. Again at 2θ value 20.2º ((020), (101)) a new peak arises in the XRD pattern, which shows the characteristic peak of the β-phase PVDF. It can be observe that for the sample S_1 the peak intensity of α-phase of PVDF is almost diminishes at 2θ =26.6º and that of the β-phase increases more. So the phase transformation from the α-phase to the electro-active β-phase of PVDF due to incorporation of the NONPs is proved.

Electron microscopy analyses

Field-emission Scanning Electron Microscopy (FESEM) and Transmission electron microscopy (TEM) images of the NiO nanoparticles and NONPS embedded PVDF films are shown in Fig. 3 and Fig. 4 respectively. Figure 4 shows the successful incorporation of the NiO nanoparticles (white spots) in PVDF matrix. Figure 5 shows high resolution TEM (HRTEM) of NiO nanoparticles are hexagonal in shape and the average diameter of the nanoparticles are 70 nm.

FTIR analysis

Fourier transform infrared (FTIR) spectrum (Fig. 6) shows the intensity versus wave number variation of the neat and nanocomposite films. In this spectrum peaks at

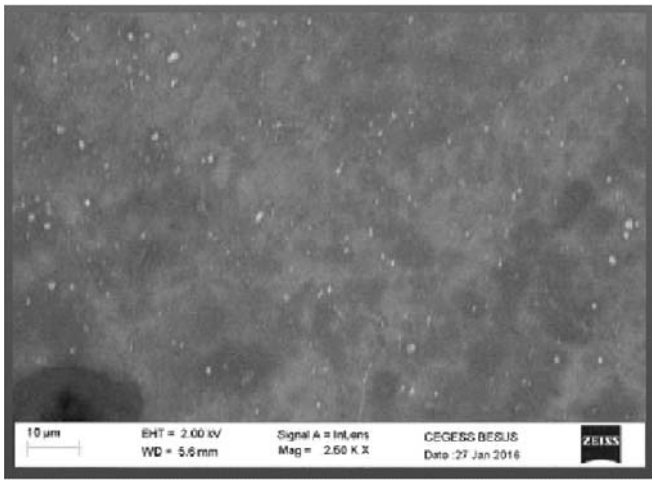

Fig. 4 TEM images of the NiO nanoparticles (white spots) embedded in PVDF.

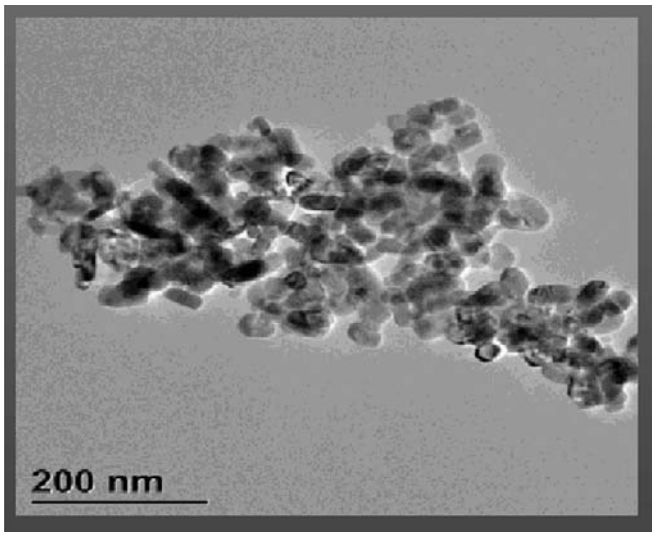

Fig. 5 HRTEM (Image) of NiO nanoparticles.

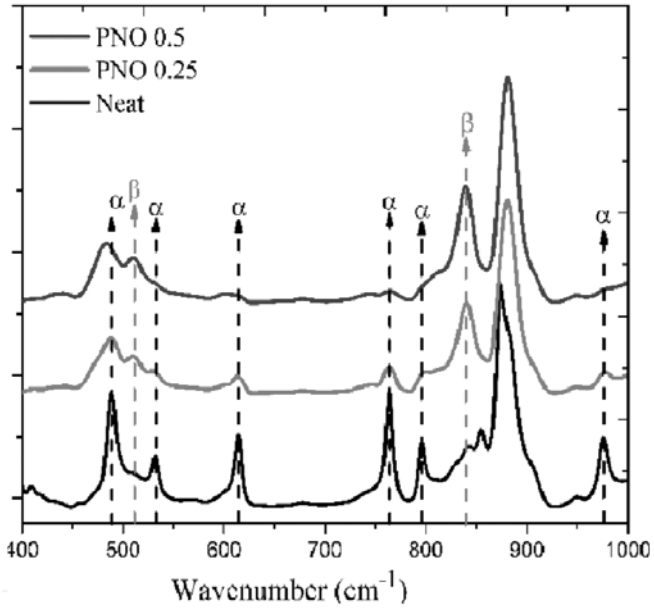

Fig. 6 Fourier transform infrared (FTIR) spectrum of the sample.

488 cm^{-1}, 532 cm^{-1}, 615 cm^{-1} and 764 cm^{-1}, 796 cm^{-1} and 976 cm^{-1} represents the IR bands of non-polar β-phase and that at 510 cm^{-1} and 840 cm^{-1} corresponding to α-phase of PVDF. From Fig. 6 it is observed that all the characteristic absorption bands corresponding to non-polar α-phase of PVDF are gradually decreasing and that to non-polar β-phase of PVDF are gradually increasing with the increase of loading fraction of NONPs in PVDF. So the transformation of α to β phase of PVDF with the loading of the NONPs in the PVDF matrix is confirmed by FTIR analysis.

Ultrasonic Measurement

i. *Comparison between wavelength of the wave and particle size:* The velocity of ultrasound[17] in PVDF matrix is in the order of $c \sim 10^3$ m/s and the order of frequency used in which this experiment has been performed $\nu \sim 10^5$ Hz. The corresponding order of the wavelength is 10^{-2} m. HRTEM image of the sample shows that the average diameter of NiO nanoparticle is 70 nm, which is much less than the order of wavelength of the ultrasonic wave used in this experiment. So it is concluded that this experiment is performed in Rayleigh Region of scattering[13-16].

ii. *Ultrasonic attenuation coefficient measurement:* Ultrasonic attenuation versus frequency graph for different concentrations of NONPs in PVDF

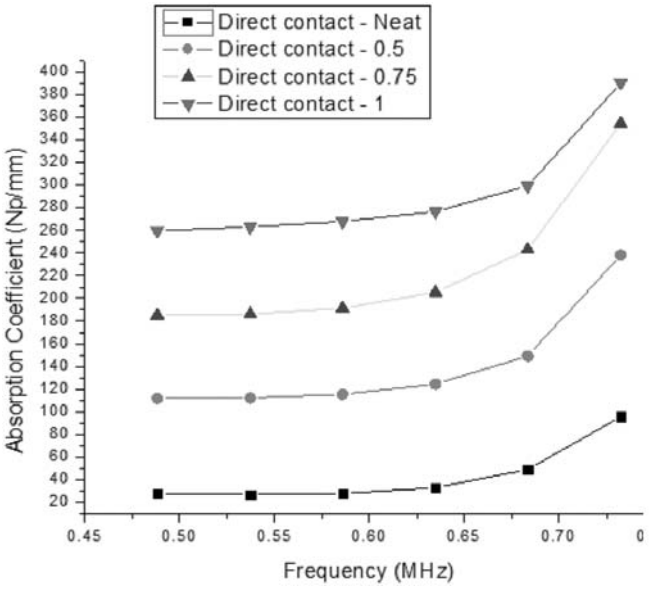

Fig. 7 Variation of Attenuation coefficient with frequency for a given concentration of the sample.

by the ultrasonic through transmission technique is as shown in the Fig. 7. Here the experiment was performed by Ultrasonic pulser/receiver instrument USLT 2000 by A-scan process[18]. The transducer of central frequency 500 kHz was used. Nature of the input pulse in time domain is shown in Fig. 8, was taken from USLT 2000 instrument software. After collecting the data from the instrument for each loading fraction of NONPs in PVDF and as well as neat PVDF, the FFT of the signals has been done for each concentration. Then attenuation coefficient is measured by using the well known formula $\alpha = (1/l) \log e (A_0/A_1)$, where α is the attenuation coefficient in neper/mm, l is the thickness of the sample in mm, A_0 and A_1 are the power emitted by the transmitter and received by receiver respectively.

The thickness of the sample is 0.250 mm, measured by digital slide calipers.

Figure 7 shows that for a given concentration of the sample, attenuation coefficient increases with the increase of frequency as the scattering increases in the Rayleigh region ($\lambda >>$ the scatterer size)[13] because the wavelength of the ultrasonic wave is very much larger than the size of the nanoparticles in this region. So the wave overlooks almost all of the particles. When we increase the frequency of the ultrasonic wave, the probability for interaction of the wave with the particle

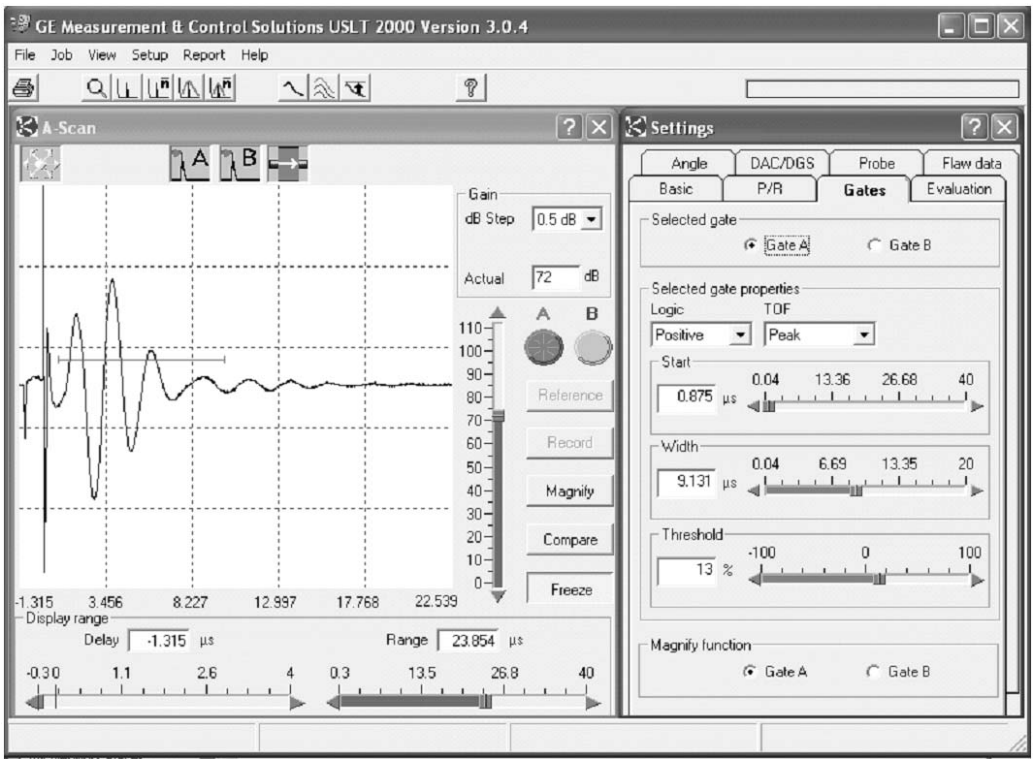

Fig. 8 Input signal pulse in time domain.

having smaller size increases. But we have not used the transducers of that frequency so that individual nanoparticle could be traced. But there is an increment of scatter density (formed due to the agglomeration of nanoparticles) and also the absorption of the wave. So, it can be supported by our experiment that with the increase of frequency the attenuation due to scattering increases.

From the Fig. 9 it can be observed that the attenuation coefficient increases with the increase of weight percent of the NiO nanoparticles in PVDF matrix due to the increase of the scattering of ultrasound by the NiO nanoparticles for a given frequency.

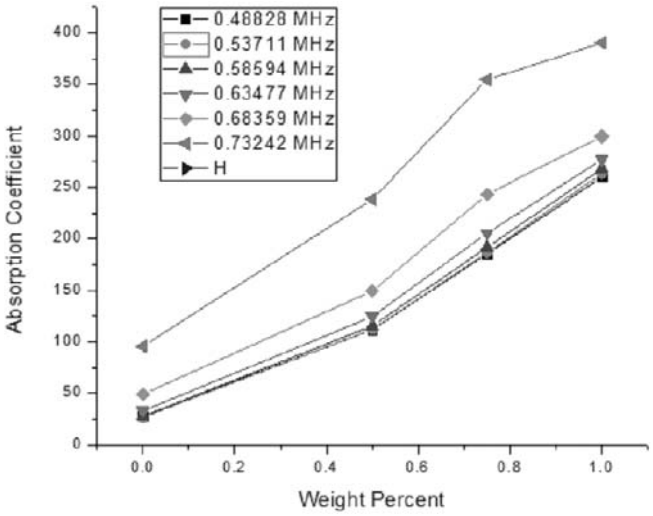

Fig. 9 Variation of Attenuation coefficient with concentration of the sample for a given frequency.

Actually the attenuation coefficient α is related with the scatter density n_0 and the scattering cross-section γ by the relation $\alpha = 1/2\, n_0\gamma$. So the attenuation coefficient increases with the increase of scatterer density depending upon the concentration of nanoparticles in the polymer matrix.

Conclusion

In this work NiO nanoparticle embedded on PVDF having different concentration as well as neat PVDF is synthesized by solution casting technique. FESEM, TEM pattern of the nanoparticle returns that synthesized NONPs are of same crystalline structure of size of the order of 70 nm. XRD, FTIR of NONPs-PVDF confirms successful phase transformation from α phase to the electroactive β phase on increasing the concentration of nanoparticles. Ultrasonic measurement of NONPs-PVDF as well as neat PVDF shows that the attenuation coefficient of ultrasonic wave increases with the frequency for a fixed concentration or loading fraction and increases with the concentration for a fixed frequency of ultrasonic wave.

Acknowledgement

This work is financially supported by NASF (ICAR), Govt. of India and Dr. Sukhen Das, Department of Physics, Jadavpur University for providing different characterization facilities.

References

1. **Jahan N., Mighri F., Rodrigue D.** and **A. Ajji**, Enhanced electroactive β-phase in three phase PVDF/$CaCO_3$/ nanoclay composites: Effect of micro-$CaCO_3$ and uniaxial stretching, *J. Appl. Polym. Sci.*, **134** (2017) 44940 (11 pp.).

2 **Dutta B., Kar E., Bose N.** and **Mukherjee S.,** Significant enhancement of the electroactive β-phase of PVDF by incorporating hydrothermally synthesized copper oxide nanoparticles, *RSC Adv.*, **5** (2015) 105422.

3 **Dutta B., Kar E., Bose N. Mukherjee N.** and **Mukherjee S.,** Poly (vinylidene fluoride)/submicron graphite platelet composite: A smart, lightweight flexible material with significantly enhanced β polymorphism, dielectric and microwave shielding properties. *Euro. Poly. J.*, **90** (2017) 442-455.

4 **Kim N.K., Richard J.T.L., Stoyko F., Kean A.** and **Bhattacharyya D.,** Nanofibrillar Poly (vinylidene fluoride): Preparation and Functional Properties, International *J. Poly. Mater. Poly. Biomater.*, **63** (2013) 23-32.

5 **Kar E., Bose N., Das S., Mukherjee N.** and **Mukherjee S.**, Enhancement of electroactive β-phase crystallization and dielectric constant of PVDF by incorporating GeO_2 and SiO_2 nanoparticles, *Phys. Chem. Chem. Phys.*, **17** (2015) 22784-22798.

6 **Martins P., Lopes A.C.** and **Lanceros-Mendez S.,** Electroactive phases of poly (vinylidene fluoride): determination, processing and applications, *Prog. Polym. Sci.*, **39** (2014) 683-706.

7 **Chang Y.M., Lee J.S.** and **Kim K.J.**, Heartbeat monitoring technique based on corona-poled PVDF

film sensor for smart apparel application. *Solid State Phenom.,* **124** (2007) 299-302.

8 **Lovinger A.J.,** Ferroelectric polymers, *Science,* **220** (1983) 1115-1121.

9 **Fukada E.,** History and recent progress in piezoelectric polymers, *IEEE Trans. Ultrason. Ferroelectr. Freq. Control,* **47** (2000) 1277-1290.

10 **He F., Fan J.** and **Lau S.** Thermal, mechanical and dielectric properties of graphite reinforced poly (vinylidene fluoride) composites. *Polym. Testing,* **27** (2008) 964-970.

11 **Balitskii D.B., Sil'vestrova O. Yu., Balitskii V.S., Pisarevskii Yu. V., Pushcharovskii D. Yu.** and **Philippot E.,** Elastic, piezoelectric, and dielectric properties of α-GeO2 single crystals. *Crystallogr. Rep.* **45** (2000) 145-147.

12 **Kozhushkoa, V.V., Paltaufa G., Krenna H., Scheriaub S.** and **Pippanb R.,** Attenuation of ultrasound in severely plastically deformed nickel. *NDT & E International,* **44** (2011) 261-266.

13 **Saniie J.** and **Bilgutay N.M.,** , Quantitative grain size evaluation using ultrasonic backscattered echoes, *J. Acoust. Soc. Am.* **80** (1986) 1816-1824.

14 **Sarpün I.H.** and **Ünal R.,** Mean grain size determination in marbles by ultrasonic techniques. *ECNDT,* (2006) - Fr.1.7.4.

15 **Hukkanen E.J.** and **Braatz R.D.,** Measurement of particle size distribution in suspension polymerization using in situ laser backscattering, *Sens. Actuators,* **B 96** (2003) 451-459

16 **Beecham D.,** Ultrasonic scatter in metals: its properties and its application to grain size determination, *Ultrasonics,* **4** (1966) 67-76.

17 **Kulkarni S.S.** and **Khadke U.V.,** Effect of solvents on the ultrasonic velocity and acoustic parameters of polyvinylidene fluoride solutions. *Ind. J. Mater. Sci.,* (2016) 9582582 (6 pp.).

18 **Keith A.W., Timothy A.S., Gary R.F., Ernest L.M., Francis C., Ernest J.F., Christopher S.H., Soo K.B., Paul L., William D. Jr O , Michael L.O., Balasundar I.R., Kirk S.K., Thaddeus A.W.** and **Jian R.Y.,** Inter laboratory comparison of ultrasonic backscatter coefficient measurements from 2 to 9 MHz. *J. Ultrasound Med.,* **24** (2005) 1235-1250.

J. Pure Appl. Ultrason. 39 (2017) pp. 55-59

Molecular interaction in N-N dimethyl acetamide and acetone at 313.15K by free volume

Rambhau Atmaramji Patil[1,*], Prashant Bhagwantrao Dabrase[2] and B.M. Suryavanshi[3]

[1]Department of Physics, S.S.S.K.R. Innani Mahavidyalaya, Karanja-444105, India
[2]Department of Physics, Bhalerao Science College, Saoner, Nagpur-441107, India
[3]Department of Physics, Government Institute of Science, Nagpur-440001, India
*E-mail: rapatil10@rediffmail.com

The ultrasonic velocity, density and viscosity of pure and binary liquid mixtures of N-N dimethylacetamide and acetone have been measured over the entire range of composition at temperature 313.15 K to evaluate the other thermo dynamical parameters such as adiabatic compressibility, intermolecular free length, free volume, internal pressure, relative association, Rao constant and Wada constant. The variation of these parameters with composition of the mixture was found to be useful in understanding the nature of intramolecular and intermolecular interactions of liquid systems. The non linearity found in all the plots of these thermodynamic parameters with the composition range indicates presence of the intermolecular interaction between the components of the unlike molecules of the mixture.

Keywords: Binary mixture, ultrasonic velocity, molecular interaction.

Introduction

Studies of ultrasonic waves play an important role in understanding the nature of the molecular interactions in pure liquid and liquid mixtures. The advances in recent years in the ultrasonic technique have become a powerful tool in evaluating information about the physical and chemical behaviour of molecules of the liquids[1-2]. The ultrasonic studies of the liquids are most preferred in many fields such as pharmaceutical industry, biomedical research, automobile industry, chemical industry, water research, scattering spectroscopy *etc.*[3]. The information of density (ρ), ultrasonic velocity (υ) and viscosity (η) of the pure liquids and their mixtures plays very important role in different applications that include surface facilities, pipeline systems & mass transfer operations by evaluating the different ultrasonic parameters[4].

In the present study the ultrasonic velocity and density with viscosity measurements have been carried out at different concentrations at temperature 313.15 K and its mixture for the determination of various thermodynamic parameters such as adiabatic compressibility (β_α), intermolecular free length (L_f), acoustic impedance (Z), free volume (V_f), internal pressure (π_i), relative association (R_A), and Rao constant (R). The variations of these parameters with concentration and temperature of binary mixtures are studied to understand molecular interactions between unlike components of the mixtures.

Experimental

Materials

The N, N-dimethyl acetamide is a chemical of Qualigens of excel grade of (99.5%) purity and Acetone is of AR grade of (99%) purity obtained commercially and used without further purifications.

Methods

The ultrasonic interferometer is a single and direct device to determine ultrasonic velocity in liquids with a high degree of accuracy within ±0.01m/s at 2 MHz. The constant temperature of the liquid inside the interferometer cell was maintained by circulating water through the outer jacket by electronically controlled thermostat with an accuracy of ±0.1°C. The densities of the binary mixtures and pure liquids were measured using

25 ml specific gravity bottle and a sensitive mono pan balance within ±0.1 mg accuracy. The viscosity of the liquids and their mixtures were measured using the suspended level viscometer. The experimentally measured ultrasonic velocity *(v)* measured in ms^{-1}, density *(ρ)* in kgm^{-3} and viscosity *(η)* in Nsm^{-2} are used to evaluate various thermo dynamical parameters like

$$\text{Adiabatic compressibility } \beta_\alpha = 1/\upsilon^2\rho \quad (1)$$

$$\text{Free length } L_f = K/\upsilon\rho^{1/2} \quad (2)$$

Where, *K* is Jacobson's constant (K=93.875 + 0.375T) $\times 10^{-8}$ and *T* being the absolute temperature

$$\text{Acoustical impedance } Z = \upsilon\rho \quad (3)$$

$$\text{Free volume } V_f = \left[\frac{Meff^{\upsilon}}{\eta k}\right]^{3/2} \quad (4)$$

Where M_{eff} is the effective molecular weight ($M_{eff} = \Sigma m_i X_i$) in which mi and X_i are the molecular weight and mole fraction of the individual constituents respectively, *k* is temperature independent constant which is equal to 4.28×10^9 for all liquids

$$\text{Internal pressure } \pi_i = \text{bRT}\left(\frac{k\eta}{\upsilon}\right)^{1/2}\left(\frac{\rho^{2/3}}{M_{eff}^{7/6}}\right) \quad (5)$$

Where *k* is a constant, *T* is the absolute temperature, b is a constant equal to 2 for the liquid and the excess values of these parameters are determined by using the relation

$$\text{Relative association } R_A = \frac{\rho}{\rho_o}\left(\frac{\upsilon_o}{\upsilon}\right)^{1/3} \quad (6)$$

$$\text{Rao constant } R = \upsilon^{1/3}.V_m \quad (7)$$

$$\text{Relaxation time } \tau = \frac{4\eta}{3\rho\nu^2} \quad (8)$$

Preparation of Samples

The binary mixtures of N, N-dimethyl acetamide and Acetone were prepared at room temperature and kept in a special airtight glass bottles to avoid air contact for different range of composition.

Results and Discussion

The measurements of ultrasonic velocity *(v)* density *(ρ)* and viscosity *(η)* at temperature 313.15 *K* have been used to calculate the different parameters such as adiabatic compressibility *(β_α)*, intermolecular free length *(L_f)*, acoustic impedance *(Z)*, free volume *(V_f)*, internal pressure *(π_i)*, relative association *(R_A)*, Rao constant *(R)*, and relaxation time *(τ)* are shown in figs. 1-2. From Fig. 1, it is observed that the ultrasonic velocity *(υ)* increases with concentration of mixture and the corresponding density also increases. As observed from the fig. 1. The values of viscosity increases with the increasing concentration and the same trend is observed for the internal pressure. The compressibility values shows decreasing trend with the increasing concentration of NN-dimethyl acetamide (NNDMA) in the mixture. The same nature as that of compressibility is also observed in the free length and in the free volume values. The increase in ultrasonic velocity may be attributed to the cohesion. The values of adiabatic compressibility *(β_α)* and free length *(L_f)* decreases with increase in the mole fraction of N-N dimethyle acetamide (Fig. 1). This suggests making and breaking of hydrogen bonding. The greater the attractive force among the molecules, the smaller will be the compressibility thus indicates formation of a complex[5]. The intermolecular free length depends upon intermolecular attractive and repulsive force. Eyring and Kincard have proposed that free length is a predominating factor in determining the variation of ultrasonic velocity of solutions[1,6,7]. The decrease in adiabatic compressibility suggests that there is significant interaction between unlike molecules of the mixture. Internal pressure of the binary mixture has non linear but increasing nature corresponding to the increasing concentration of NNDMA in the binary mixture. The increases in internal pressure may be due to various degrees of dispersive interactions and Columbic interactions existing between the component molecules[8]. The free volume values corresponding to the increasing concentration of the NNDMA in the binary mixture of NNDMA and Acetone are decreases. The decrease in free volume indicates the molecules are coming closure and the fact is conformed from the free length values, which conforms the increasing magnitude of the interaction. The non linear variation is an indication of existence of interaction between the components of the mixture[9-10].

Acoustic impedance of a material is the opposition exerted by the medium to displacement of particles in the medium by the sound energy. The value of acoustical impedance increases with the increase in concentration of the NNDMA in the binary mixture of NNDMA and

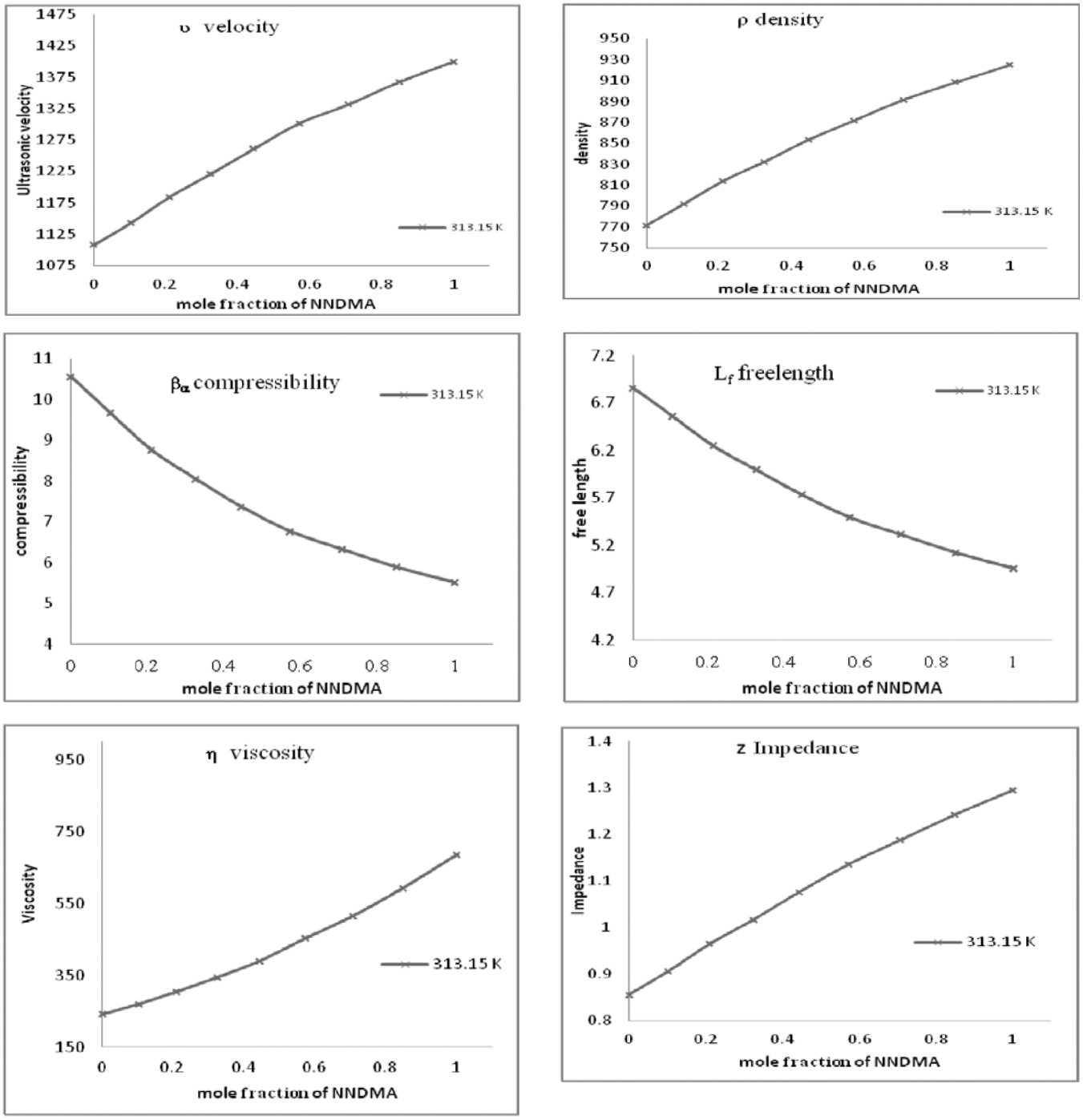

Fig. 1 Graph of ultrasonic velocity *(υ)*, density *(ρ)*, compressibility *(β_α)*, free length *(L_ρ)*, impedance *(Z)* and viscosity *(η)* of NNDMA + acetone mixture with respect to concentration of NNDMA in Acetone mixture at 313.15 K.

acetone. This non-linearly supports the strong molecular interactions as suggested by Oswal *et al.*,[11]. When an acoustic wave travels in a medium, there is a variation of pressure and instantaneous velocity from particle to particle. This is governed by the inertial and elastic properties of the medium.

The viscosity values are increasing with the increasing concentration of NNDMA in the mixture. The increase in values of viscosity with increase in mole fraction of N, N-dimethyl acetamide suggests the increase in magnitude of intermolecular interactions as reported by Palaniappan[12].

The values of relative association R_A increases [Fig. 1] with the increase in mole fraction of NNDMA in the binary mixture, this increase in relative association indicates the presence of molecular interaction between unlike molecules. Such increase in relative association supports the idea that the liquid system is in a more compressed state and the component molecules are much closer to each other at higher concentration of NNDMA and there may exist dipole-induced dipole interactions between component molecules in the binary liquid mixture. From Fig. 2, the Rao Constant *R* (The molar sound velocity) and Wada constant *W* (molar compressibility) increase linearly with the increase in mole fraction of NNDMA in the binary mixture of NNDMA and acetone systems, indicating the presence of specific interactions in the binary liquid mixture without complex formation[13], solute-solvent interactions[14]. According to Kannappan *et al.*[15], this suggests the presence of intermolecular interaction in the systems. As the system is polar-nonpolar or polar-polar type so the possible heteromolecular association may be due to dipole-induced-dipole or dipole-dipole interaction.

The order of relaxation time is of 10^{-12} s which is due to the structural relaxation process and such type of situation is due to rearrangement of the molecules

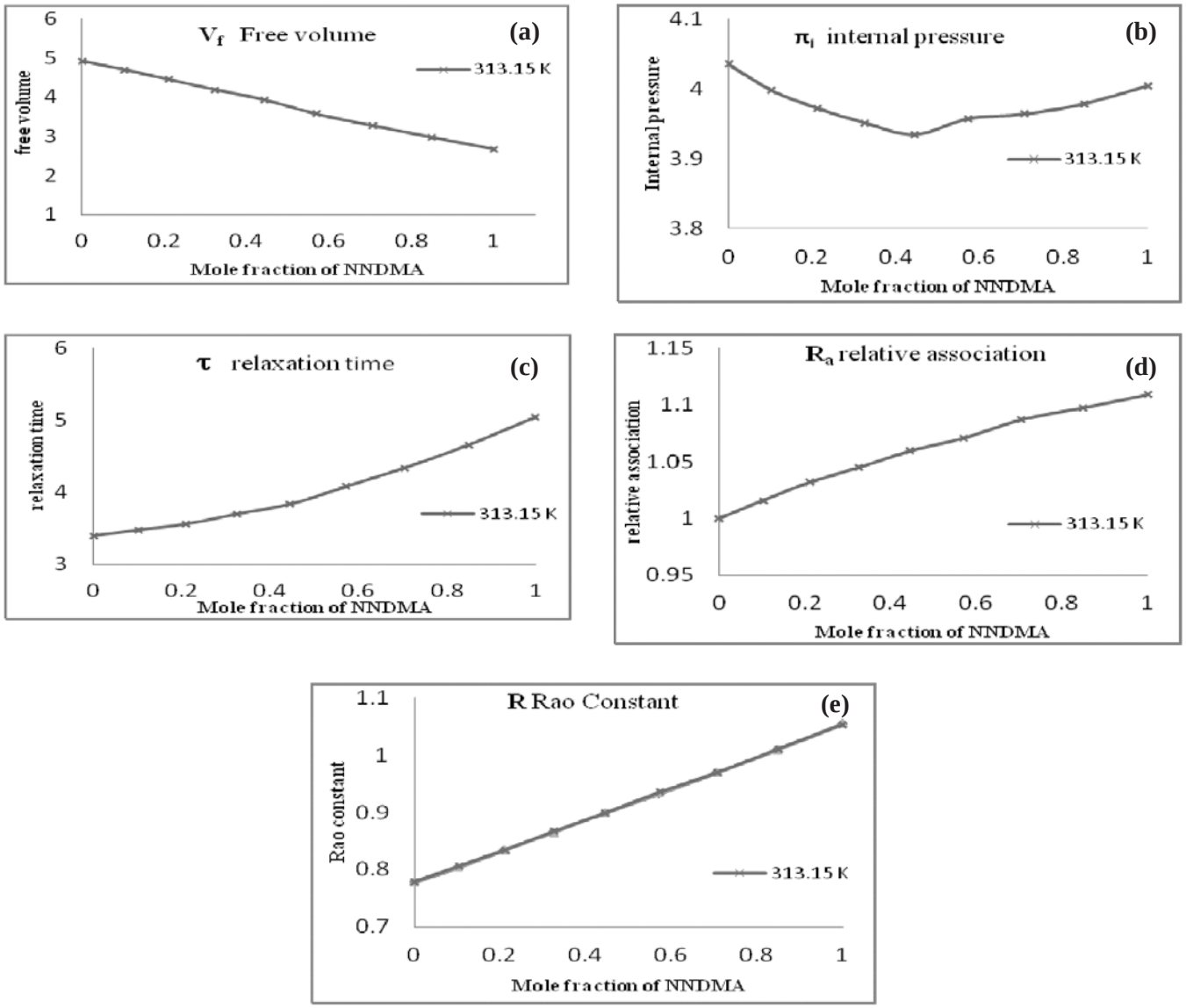

Fig. 2 Graph of free volume *(V_f)*, internal pressure *(π_i)*, relaxation time *(τ)*, relative association *(R_A)*, Rao's constant *(R)* of NNDM + acetone mixture with respect to concentration of NNDMA in Acetone mixture at 313.15 K.

because of cooperative process. The non linear variations in the relaxation time with the mole fraction are interpreted as possible molecular association between the molecules of NNDMA and acetone in the mixture[16].

Conclusion

The ultrasonic velocity, density and viscosity measurements have been carried out for determination of ultrasonic parameters such as compressibility (β_α) molecular free length (L_f), free volume (V_f) and internal pressure (π_i), Rao's constant *(R)* for the different composition range of NN-dimethyacetamide in acetone at the temperatures 313.15K.

The present investigations lead us to conclude that the presence of strong dispersive dipole-dipole interaction between the components of molecules in the mixture. The non-linearity of the curve and Rao's constant and Wada constant also supports the interaction exists in the systems.

Acknowledgements

The authors are thankful to the Director and Head Department of Physics, Government Institute of Science, Nagpur, and the Principal, S.S.S.K.R. Innani M.V., Karanja (lad) authorities for providing the facilities to carry out this work.

References

1 **Eyring H.** and **Kincaid J.F.,** Free volumes and free angles ratios of molecules in liquids, *J. Chem. Phys.,* **6** (1938) 620-629.

2 **Pitzer K.S.,** Thermodynamics, 3rd edition McGraw-Hill, New York, 1995.

3 **Pandey J.D., Dey R.** and **Bhatt B.D.** Applicability of thermoacoustical parameters for the computation of available volume in liquid systems, *Phys. Chem. Comm*., **5** (2002) 37.

4 **Dabrase P.B., Patil R.A.** and **Suryavanshi B.M.,** Intermolecular interactions in NN dimethyl acetamide and acetone at different temperatures, Applied Ultrasonics, Shree Publishers, New Delhi, (2012) pp.233-241.

5 **Varma R.P.** and **Surendra Kumar,** Ultrasonic velocity and density measurements of ammonium soaps in 2-propanol with ketones, *Indian J. Pure Appl. Phys.,* **38**, (2000) 96-100.

6 **Rajgopal K.** and **Chenthilnath S.**, Excess thermodynamic studies of binary mixtures of 2-methyl-2-propanol with ketones, *Indian J. Pure Appl. Phys.,* **48** (2010) 326-333.

7 **Kannappan A.N.** and **Rajendran V.,** Molecular interaction studies in temary liquid mixtures from ultrasonic data, *Indian J. Pure Appl. Phys.,* **29** (1991) 465-468.

8 **Praharaj M.K., Satapathy A., Mishra S.** and **Mishra P.R.,** Study of thermodynamic and transport properties of ternary liquid mixture at different frequencies, *J. Chem. Pharma. Res.,* **4**(4) (2012) 1910-1920.

9 **Ali A.** and **Nain A.K.**, Ultrasonic study of molecular interaction in Binary liquid mixtures at 303.15K, *J. Pure Appl. Ultrason.,* **21** (1999) 31-34.

10 **Patil R.A., Dabrase P.B.** and **Suryavanshi B.M.,** Excess Thermodynamic Properties of Binary Liquid Mixture of N, N-dimethylacetamide in Benzonitrile through Ultrasonic measurements at 308.15 K, *Int. J. of Sc. Res.*, (2015) 232-235.

11 **Oswal S.L., Oswal P.** and **Pathak R.P.,** Physico-chemical behavior of binary and ternary liquid mixtures, *J. Sol. Chem.* **27** (1998) 507-511.

12 **Palaniappan L.,** Thermo acoustical studies of some iso-alcohols in cyclohexane with toluene, *Indian J. Pure Appl. Phys.,* **40** (2002), 828-830.

13 **Dash Ashok Kumar** and **Paikaray Rita,** Study of molecular interaction in binary liquid mixture of dimethyl acetamide and acetone using ultrasonic probe, *Adv. Appl. Sc. Res.,* **4**(3) (2013) 130-139

14 **Baluja S.** and **Oza S.**, Study of some acoustical properties in binary solution, *Fluid Phase Equilibr.,* **178** (2002) 233-238.

15 **Kannappan, A.N.** and **Palani R.,** Studies on molecular interaction in ternary liquid mixtures by ultrasonic velocity measurements, *Ind. J. Phy. B,* **70** (1996) 59-65.

16 **Ali S. Hyder** and **Nain A.K.,** Intermolecular interactions in ternary liquid mixtures by ultrasonic velocity measurements, *J. Phy.,* **74**(B1) (2000) 63-67.

J. Pure Appl. Ultrason. 39 (2017) pp. 60-69

Computation of erosion potential of cavitation bubble in an ultrasonic pressure field

B.K Sreedhar[1,*], S.K. Albert[2] and A.B Pandit[3]

[1]Fast Reactor Technology Group, Indira Gandhi Centre for Atomic Research,
Homi Bhabha National Institute, Kalpakkam-603102, India
[2]Materials Technology Division, Metallurgy and Materials Group, Indira Gandhi Centre for Atomic Research,
Homi Bhabha National Institute, Kalpakkam-603102, India
[3]Department of Chemical Engineering, Institute of Chemical Technology, Mumbai-400019, India
*E-mail: bksd@igcar.gov.in

Cavitation is the creation and collapse of a vapor cavity in a liquid. Cavitation can be produced by a sound field and this principle is employed in the ultrasonic vibratory cavitation device. The rapidly fluctuating applied pressure results in cavitation of the liquid. The pressure produced by the collapse of a vapor bubble can be determined by solving equations of bubble dynamics. The fundamental equation of bubble dynamics is the Rayleigh-Plesset-Noltingk-Neppiras-Poritsky equation popularly known as the RP equation. This equation does not account for the effect of liquid compressibility. Gilmore's equation, which considers liquid compressibility, can be used to obtain realistic estimates of bubble wall velocities at the end of bubble collapse. This paper discusses the numerical solution of Gilmore's equation to evaluate the bubble wall velocity at the end of bubble collapse and the pressure imposed on a solid surface from impingement of the resulting jet. The parameters affecting the growth and collapse of a single bubble is are studied. A discussion of results of cavitation damage experiments in sodium is also provided as a confirmation of the theoretical estimate of damage.

Keywords: Ultrasonic cavitation, Gilmore's equation, collapse pressure

Introduction

Cavitation is a phenomenon which occurs in liquid systems when the static pressure at any point in the system falls below the vapor pressure at constant system temperature. It is therefore the process of boiling in the liquid due to pressure reduction rather than heat addition. In a flowing system the pressure reduction can occur due to hydrodynamic effect and the resultant two phase flow is known as cavitating flow. The vapor bubbles thus formed, in the regions of minimum pressure, are carried by the flowing liquid to eventually collapse in regions where the pressure recovers and exceeds the vapor pressure. The collapse can result in noise and vibrations and can lead to severe damage of the metal surface if the collapse occurs adjacent to the metal surface. In hydraulic machinery this results in performance degradation and component damage. It is therefore the goal of a designer to avoid cavitation during the expected range of operation of the equipment. However, in the case of complex and capital intensive engineering systems like a nuclear reactor it is not always possible to avoid cavitation altogether during normal operation from economic considerations.

Systematic studies on cavitation damage are therefore important to obtain valuable basic and applied data of direct use.

Mechanism of erosion damage

Cavitation damage results from the impulsive pressures producing from collapsing bubbles. The impulsive pressure is produced in one of two ways *viz.* (i) through a shock wave, or (ii) by means of a micro jet. A bubble containing a mixture of gas and vapor expands from its initial radius, R_0, during a rarefaction and then collapses under the influence of a pressure peak. If the bubble is

adjacent to a solid boundary the collapse is asymmetric and results in the formation of high velocity micro jets. Damage results from the impingement of these microjets with the solid surface.

In the case of a collapsing bubble in the bulk liquid and away from solid boundaries the collapse is initially symmetric (in the final stages of collapse, however, the spherical form becomes unstable[1]). During this process the bubble contents are compressed to vey high values of pressure and temperature. The increasing pressure of the bubble contents stops the radially inwards moving bubble wall and causes the bubble to rebound and a pressure transient to be generated that evolves into a shock wave front. The interaction of this wave front with a solid boundary results in damage to the solid surface.

In a real system the cavitation cloud consists of bubble clusters of large numbers of bubbles of varying sizes that affect the pressure driving bubble collapse as well as the damping/cushioning effect of the resulting impact pressure. This paper, however, discusses the erosion potential of a single bubble.

Equations of bubble collapse

The theoretical treatment of cavitation invariably begins with the equations of bubble collapse formulated by Rayleigh[2]. Rayleigh considered the symmetrical collapse of an empty spherical cavity in an infinite body of incompressible liquid under constant pressure. By equating the work done on the system (*i.e.* liquid and empty cavity) by the constant external pressure to the kinetic energy *(KE)* gained by the liquid, the expression for the velocity of the cavity wall was obtained

$$U^2 = \frac{2P}{3\rho}\left(\frac{R_0^3}{R^3} - 1\right) \qquad (1)$$

where ρ = density of the liquid, R = bubble radius at any instant of time, R_0 = initial bubble radius, P = pressure at infinity driving collapse, U = bubble wall velocity = $\frac{dR}{dt}$. Equation (1) shows an unlimited increase of velocity as $R \geq 0$. Rayleigh was aware of the problem and resolved the issue by explaining that in reality there will be insoluble gas in the cavity.

Considering the isothermal compression of a gas filled cavity and equating the work done on the system (*i.e.* liquid and gas filled cavity) to the sum of the kinetic energy of the liquid and the work done in compressing the gas, Rayleigh formulated an expression for the velocity of the bubble wall as a function of the bubble radius. The equation was improved by Plesset[3], Noltingk and Neppiras[4] and Poritsky[5] to give the now famous Rayleigh-Plesset equation

$$R\ddot{R} + \frac{3}{2}\dot{R}^2 = \left\{\frac{1}{\rho}P_{v\rho} - P_\infty(t) + P_{g0}\left(\frac{R_0}{R}\right)3\gamma - 2\frac{\sigma}{R} - 4\mu\frac{\dot{R}}{R}\right\} \qquad (2)$$

where $P_{v\rho}$ = vapor pressure of the liquid, $P_\infty(t)$ = pressure at infinity in the liquid, P_{g0} = initial pressure of gas in the liquid, σ = surface tension of the liquid, μ = viscosity of the liquid.

Equation (2) has been derived with the following assumptions, *viz.* the bubble is spherical during the entire collapse process, the liquid is incompressible, no body forces exist, conditions within the bubble are spatially uniform and the gas content in the bubble is constant.

In reality, bubble collapse is rapid and liquid compressibility is to be considered. Flynn[6] discusses other forms of the above equation which take the compressibility of liquid into consideration. The simplest is the acoustic approximation in which the speed of sound is considered constant and this limits its use to cases where the bubble wall velocity is small compared to the speed of sound. The loss of energy due to sound radiation is considered in this analysis. The acoustic approximation equation is given by

$$R\ddot{R} + \frac{3}{2}\dot{R}^2 = \frac{1}{\rho}\left\{P_L + \frac{R}{C}\left(1 - \frac{\dot{R}}{C}\right)\frac{dPL}{dt} - P_\infty(t)\right\} \qquad (3)$$

The Herring[7] approximation incorporates a more satisfactory description of the energy loss through compression of the liquid and sound radiation. It is given by

$$\left(1 - \frac{2\dot{R}}{C}\right)R\ddot{R} + \frac{3}{2}\left(1 - \frac{4\dot{R}}{3C}\right)\dot{R}^2 = \frac{1}{\rho}\left\{P_L + \frac{R}{C}\left(1 - \frac{\dot{R}}{C}\right)\frac{dPL}{dt} - P_\infty(t)\right\} \qquad (4)$$

A more complete description is provided by Gilmore[8] who considers the formation of shock waves when the bubble wall velocity approaches the velocity of sound. This is achieved using the Kirkwood-Bethe hypothesis which states that the shock waves are propagated with a velocity equal to the sum of the sound velocity and the fluid velocity. Gilmore's equation is

$$\left(1 - \frac{\dot{R}}{C}\right)R\ddot{R} + \frac{3}{2}\left(1 - \frac{\dot{R}}{3C}\right)\dot{R}^2 = \left(1 - \frac{\dot{R}}{C}\right)H + \frac{R}{C}\left(1 - \frac{\dot{R}}{C}\right)\frac{dH}{dt} \qquad (5)$$

The paper discusses the solution of the Gilmore

equation for a single bubble and the influence of various parameters on the damage pressure.

Solution of Gilmore's equation

The pressure in the liquid at the bubble interface, P_L is specified as a function of t or R and H and C are related to P_L using an equation of state for liquids. For most liquids the pressure-density curve for adiabatic compression can be expressed using the relation known as Tait's equation of state[9], *viz.*

$$\frac{p+B}{p_\infty+B}=\left(\frac{\rho}{\rho_\infty}\right)^n \tag{6}$$

where ρ = density of the liquid, p = pressure of the liquid, n = index, subscript ∞ refers to the initial condition, B is a constant for a liquid and nB is the compressibility coefficient given by the expression, $nB=\frac{1}{\rho}\frac{dp}{d\rho}$.

The liquid enthalpy is given by the expression[10],

$$H=\int_{\rho_\infty}^{p_L}\frac{dp}{d\rho} \tag{7}$$

From Eq. (6), $\rho=\left(\frac{p+B}{p_\infty+B}\right)^{\frac{1}{n}}\rho_\infty$.

Sub for ρ in Eq. (7), $H=\frac{A^{\frac{1}{n}}}{\rho_0}\int_{P_\infty}^{P_L}(p+B)^{\frac{-1}{n}}dp$.

$$H=\frac{n}{n-1}\frac{A^{\frac{1}{n}}}{\rho_0}\left((P_L+B)^{\frac{n-1}{n}}-(P_\infty+B)^{\frac{n-1}{n}}\right) \tag{8}$$

where P_L = pressure in the liquid at the bubble wall

$$=P_{v\rho}+P_{g0}\left(\frac{R_0}{R}\right)3\gamma-\frac{2\sigma}{R}-4\mu\frac{\dot{R}}{R}$$

The local velocity of sound in the liquid[10],

$$C=\sqrt{\frac{\partial P}{\partial\rho}} \tag{9}$$

Using equation Eq. (9),

$$C^2=\frac{\partial P}{\partial\rho}=\frac{(P_\infty+B)n\rho^{n-1}}{\rho_0^n}$$

$$(P_\infty+B)\left(\frac{\rho}{\rho_0}\right)^{n-1}\left(\frac{n}{\rho_0}\right)=C_0^2\left(\frac{\rho}{\rho_0}\right)^{n-1} \tag{10}$$

where

$$C_0^2=(P_\infty+B)\left(\frac{n}{\rho_0}\right) \tag{11}$$

is the absolute velocity of sound in the liquid.

The expression for liquid enthalpy can also be written in terms of the absolute velocity of sound in the liquid and the local and absolute liquid densities.

Using Eq. (7), $H=\int_{p_\infty}^{P_L}\frac{dp}{\rho}$

Substituting for dP from Eq. (10)

$$H=\int_{\rho_\infty}^{\rho}C_0^2\left(\frac{\rho}{\rho_0}\right)^{n-1}\frac{\partial\rho}{\rho}=\frac{C_0^2}{n-1}\left[\left(\frac{\rho}{\rho_0}\right)^{n-1}-1\right] \tag{12}$$

Substituting for $\left(\frac{\rho}{\rho_0}\right)^{n-1}$, from Eq. (10), in Eq. (12),

we get $H=\frac{C^2-C_0^2}{(n-1)C_0^2}$.

Therefore, $$C=\left(C_0^2+(n-1)H\right)^{\frac{1}{2}} \tag{13}$$

Gilmore's Eq. (5) is solved simultaneously with Eqs. (8) and (13) using the 4th order Runge Kutta method.

Estimation of pressure due to liquid jet impingement

In the case of a bubble collapsing on a solid surface the jet of liquid produced from the collapsing bubble impinges on the surface directly and produces damage. The jet velocity is obtained by solution of the Gilmore equation (or *RP* equation for the case of incompressible liquid). It is assumed that at the instant the liquid jet comes into contact with the solid surface the kinetic energy of each particle of the jet is converted to elastic deformation of the same particle as determined by the bulk modulus of elasticity of the liquid. The instantaneous pressure P' on the solid surface is then obtained using the relation[2, 11].

$$\frac{p'^2}{2E}=\frac{1}{2}\rho U^2 \tag{14}$$

where

P' = instantaneous pressure on the solid surface, Pa,

E = modulus of elasticity of sodium (water), Pa

U = jet velocity at the end of bubble collapse, m/s

Estimation of pressure due to bubble collapse from shock waves

During collapse of a bubble the pressure at the interface can attain extremely large values radiating spherical waves which are converted into shock waves as they propagate through the liquid. According to the Kirkwood Bethe hypothesis in the case of spherical waves of finite amplitude the quantity $r\varphi$ propagates with a velocity $C' = C + U$ where C is the local velocity of sound in the liquid and U is the local liquid velocity. In addition to this the quantity $G = r\frac{\partial \phi}{\partial t}$ is also propagated with velocity C'. It is seen from the continuity equation and the equation of motion[10] that $\frac{\partial \phi}{\partial t} = h + \frac{u^2}{2}$.

Therefore, $$G(r,t) = r\left(h + \frac{u^2}{2}\right) \qquad (15)$$

The quantity G is propagated with velocity C'. Hence if the value of $G(R, t_R)$ is known at the surface of a radiating sphere of radius R at time t_R, its value at any other radius r can be determined from the condition $G(R, t_R) = G(r, t)$ where $t = t_R + \int_R^r \frac{dr}{C'}$

From Eq. (15) it may be concluded that

$$G(R, t_R) = R\left(H + \frac{U^2}{2}\right) \qquad (16)$$

where H and U are obtained from the solution of Eq. (16). The value of G at any point r in the liquid is determined by the value of the pressure p at that point.

The value of the pressure P at any point r is given by the equation[10]

$$P = A\left[\frac{2}{n+1} + \frac{n-1}{n+1}\left(1 + \frac{n+1}{rC_0^2}G\right)^{1/2}\right]^{\frac{2n}{n+1}} - B \qquad (17)$$

Calculation of collapse pressure from single bubble collapse in sodium

According to Flynn[6] the upper limit on the size of free nuclei in water is 2×10^{-2} cm (200 μm) whereas the size of free nuclei in fresh drawn tap water that is allowed to stand for a few seconds is 5×10^{-3} cm (50 μm).

Assuming the same initial bubble size of 200 μm *i.e* R_0 = 200 μm) in sodium and $\frac{dR}{dt_{t=0}} = 0$ the bubble variation is computed using Gilmore's Eq. (5).

For sodium at 400ºC, the properties[12] are - vapor pressure = 78.2 Pa, density = 858 kg/m^3, surface tension = 0.169 N/m, viscosity = 2.79×10^{-4} Pa-s, surface tension = 0.169 N/m); adiabatic compressibility of liquid sodium, β_0, at 400ºC, is 2.09×10^{-10} m^2/N, modulus of elasticity, $E = 1/\beta = 4.79\times10^9$ N/m^2.

In vibratory cavitation, the horn vibrates at a frequency, ω = 20 kHz, with peak to peak amplitude of 25 μm.

The operating parameters are : acoustic amplitude[1], P_a = 31,8*10^5 Pa, frequency of horn = ω = 2*π*20000, atmospheric pressure, P_{atm} = 1*10^5, speed of sound in sodium, C_0 = 2361 m/s. The index 'n' for liquid sodium in Tait's equation of state (6) is, from[13], n = 4.002,

The constant B = $\frac{1}{n\beta_0}$. B = $\frac{1}{4.002(2.09\times10^{-10})}$ = 1.196×10^9 N/m^2

Speed of sound in liquid sodium[12],

$$C_0 = \sqrt{\frac{1}{\rho\beta_0}} = \sqrt{\frac{1}{858\times2.09\times10^{-10}}} = 2361 \text{ m/s}$$

Figure 1 shows bubble radius with time

The values of the bubble radii, at the beginning and end of collapse, and the maximum bubble wall velocity during collapse are 1.33 mm, 17.9 μm and 1897 m/s respectively. The collapse pressure generated from the impingement of jet at the end of collapse with the solid boundary is calculated (from Eq. 14) to be 3846 MPa.

The pressure resulting from the rebound of the high pressure gas/vapor bubble at the end of collapse is calculated using 17 and is shown in Fig. 2.

Although the pressure at the bubble wall is of the order of 10^{10} N/m^2, the pressure drops quickly away from the

In vibratory cavitation, the horn vibrates at a frequency, ω = 20kHz with peak to peak amplitude of 25μm. The applied pressure is a sinusoidal wave $P_a \sin(\omega t)$, The acoustic amplitude, $P_a = V C_0$. The velocity $\upsilon = A\omega$ where A = peak- peak amplitude / 2 = $25\times10^{-6}/2 = 12.5\times10^{-6}$ m, and $\omega = 2\times\pi\times20000 = 125.67\times10^3$, C_0 = speed of sound in sodium =2361 m/s for water

Therefore, $P_a = \rho V C_0 = 858\times(125.67\times103\times12.5\times10^{-6})\times2361 = 31.8\times10^5$ Pa.

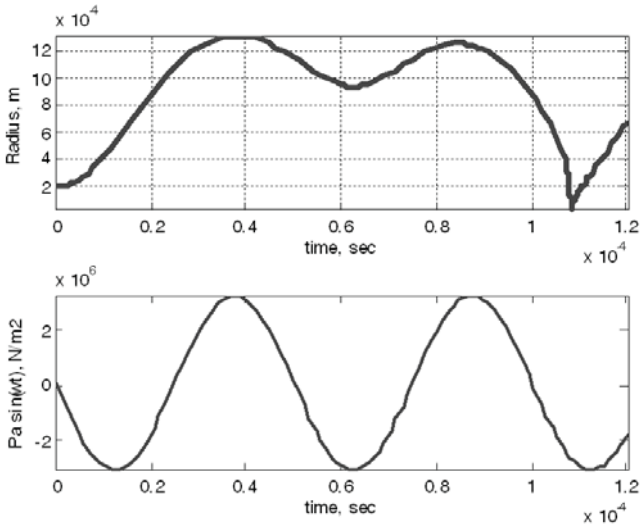

Fig. 1 Variation of bubble radius with time in sodium (R_0 = 200 μm, f = 20 kHz, peak to peak amplitude = 25 μm, $\left(\frac{dR}{dt}\right)_{t=0}$ P_a = 31.8*10^5 P_a, T = 400°C).

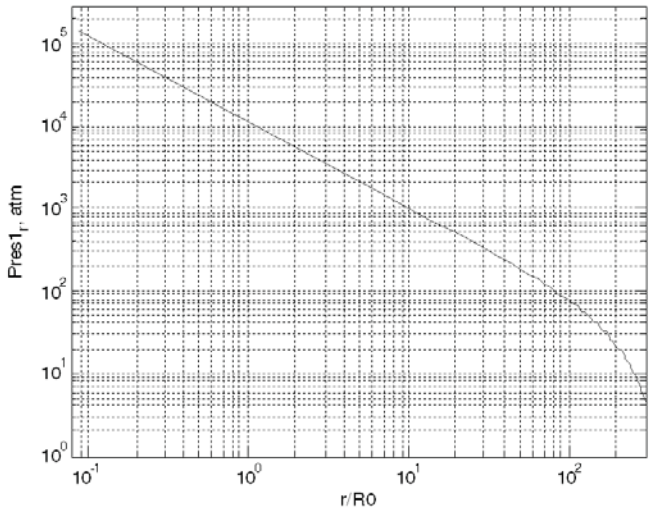

Fig. 2 Variation of pressure in sodium with radial distance from the collapse center

bubble wall and is still high enough to cause damage at a distance of about 2 times the original bubble radius. In reality there will be an additional decrease due to irreversible thermodynamic losses at the shock wave front[10]. Hence the radial extent of damaging pressure value will be less than 2 times the original radius.

Parametric study

A parametric study was carried out to examine the influence of various parameters (test and fluid) on the erosion damage.

Effect of initial bubble size

Table 1 give the effect of the initial bubble size on the estimated collapse pressure from jet impingement.

The resonance bubble size for the operating frequency of 20 kHz is 150 μm. Bubbles less than or equal to the resonant size are referred to as transient bubbles and they collapse violently[14]. Bubbles large than the resonant size are referred to as stable bubbles and these bubbles oscillate over few cycles before collapsing. This accounts for the large impact pressures for bubble sizes ≤ 150 μm.

Effect of peak to peak amplitude

Table 2 gives the effect of the peak to peak amplitude on the damage pressure.

The acoustic pressure is directly proportional to the peak to peak amplitude. Increasing the peak to peak amplitude of vibration therefore increases the acoustic pressure amplitude P_a. This lengthens the expansion phase and increases the bubble size at the end of expansion as well as the time at the end of expansion and the collapse time, Δt. However, beyond a limit the collapse time exceeds half the period, T/2 (*i.e.* the period during which the imposed pressure field is high) and the bubble degenerates into a pulsating bubble and the jet velocity at the end of collapse decreases (as seen in Table 3, cases 3 & 4 and Fig. 3, cases c & d).

Table 1 – Effect of initial bubble size on collapse pressure.

Peak to peak = 25 μm, Sodium temp, T = 400°C, $\left(\frac{dR}{dt}\right)_{t=0}$ = 0

Initial bubble size, μm	Max bubble size, mm	Min. bubble size, μm	Velocity of jet, m/s	Impact pressure, MPa
100	1.27	7.1	4582	9289
150	1.30	11	3171	6429
200	1.33	17.9	1897	3846

Table 2 – Effect of peak to peak amplitude on collapse pressure.

Initial bubble size = 200 μm, Sodium temp, T = 400°C, $\left.\frac{dR}{dt}\right|_{t=0} = 0$

Peak to peak amplitude, μm	Max bubble size, mm	Min. bubble size, μm	Collapse time, μs	Velocity of jet, m/s	Impact pressure, MPa
10	0.85	19.8	16	1077	2183
25	1.33	17.9	24	1897	3846
40	1.66	25.7	29	1191	2415
50	1.85	66.5	36	197	398

P-P = 10 μm

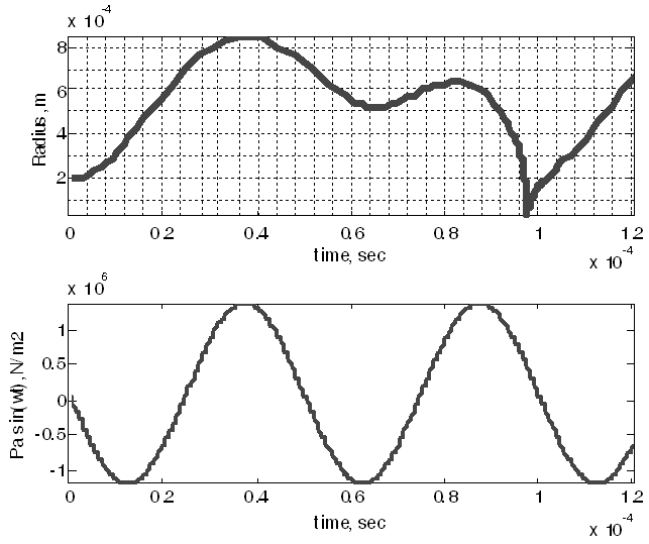

R_{max} = 0.85 mm, R_{min} = 19.8 μm, t = 16 μs,
T/2 = 25 μs P_{col} = 2183 MPa

(a)

P-P = 25 μm

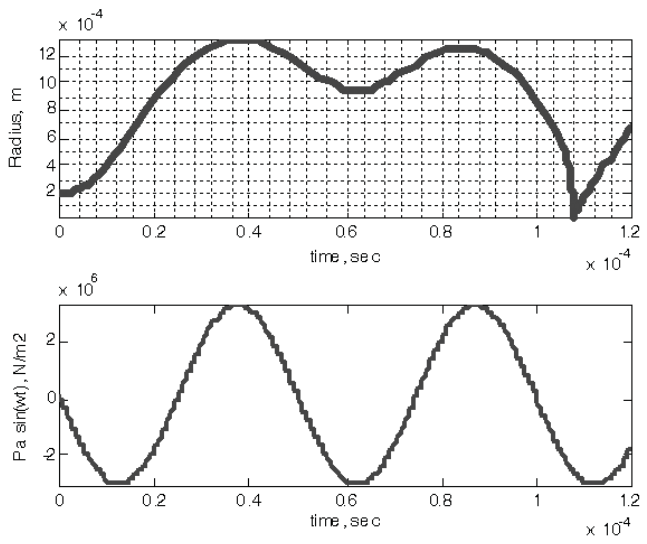

R_{max} = 1.33 mm, R_{min} = 17.9 μm, t = 24 μs,
T/2 = 25 μs P_{col} = 3846 MPa

(b)

P-P = 40 μm

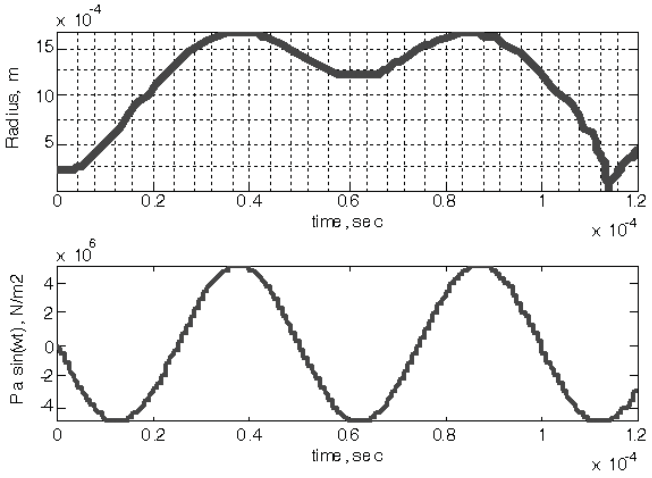

R_{max} = 1.66 mm, R_{min} = 25.7 μm, t = 29 μs,
T/2 = 25 μs P_{col} = 2415 MPa

(c)

P-P = 50 μm

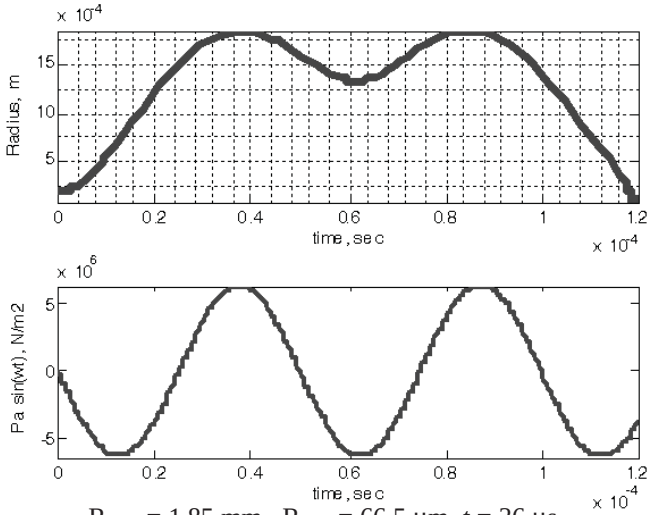

R_{max} = 1.85 mm, R_{min} = 66.5 μm, t = 36 μs,
T/2 = 25 μs P_{col} = 398 MPa

(d)

Fig. 3 Bubble radius variation for different values of peak to peak amplitude

Effect of frequency

Table 3 give the effect of frequency on the damage pressure.

Table 3 – Effect of frequency on collapse pressure.

Initial bubble size = 200 μm, Sodium temp, T = 400°C, $\left.\frac{dR}{dt}\right|_{t=0} = 0$

Frequency kHz	R_{max} mm	R_{min} μm	V m/s	Collapse pressure, MPa
20	1.32	17.9	1897	3846
40	1.05	14.2	2333	4731
100	0.798	13.8	2019	4092
500	0.63	576	201	407

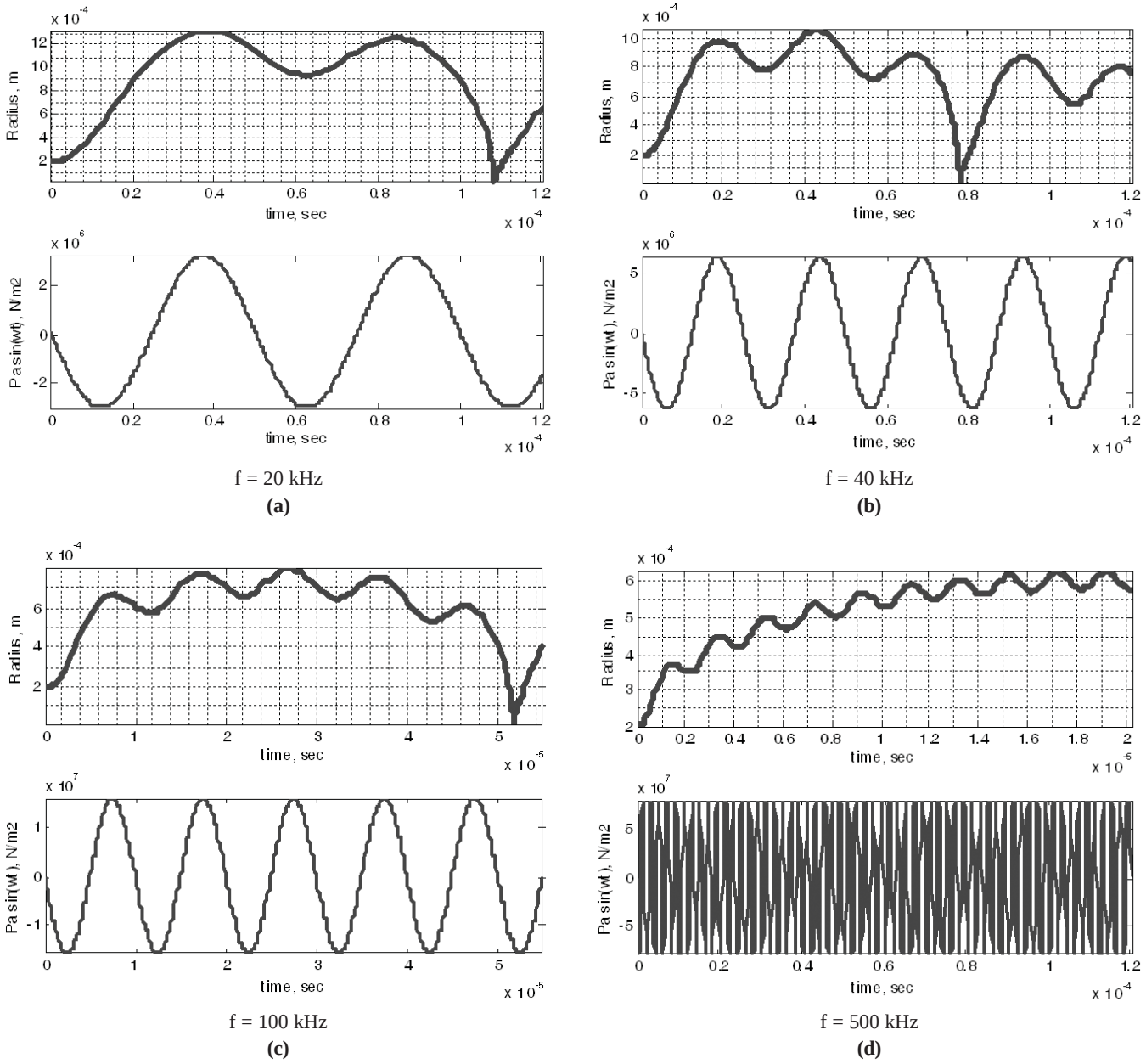

Fig. 4 Effect of frequency on collapse pressure.

Increasing the oscillation frequency reduces the maximum bubble radius at the end of expansion because the time available for expansion of the bubble decreases with increasing frequency. This results in higher pressure of vapor gas mixture inside the bubble at the beginning of collapse which reduces the bubble wall velocity at the end of collapse. At very large frequency the bubble becomes a pulsating bubble as shown in Fig. 4(d).

Effect of liquid temperature

Table 4 below gives the effect of liquid temperature on the damage pressure. The fluid properties that influence bubble formation and collapse which are considered in solving Gilmore's equation are: density, viscosity, surface tension, vapor pressure and compressibility. The solution of Gilmore equation shows that the net effect is an initial increase and then decrease in damage intensity.

The above calculations do not account for the effects of heat transfer and differences in specific volume between vapor and liquid which are expected to reduce the intensity of damage as the liquid temperature approaches the boiling point.

Comparison of damage in sodium with that in water

The liquid properties that affect collapse intensity are density, vapor pressure, compressibility, viscosity, surface tension, gas content and thermodynamic properties such as latent heat, thermal conductivity, specific heat *etc.*[15].

The damage intensity in sodium at 400ºC is compared with that of water at 20ºC. There is not much difference between the density and viscosity of water and sodium. However, the large differences between the vapor pressure, dissolved gas content and sonic velocity in sodium and water results in much higher cavitation collapse pressure in sodium than in water.

Experimental results with vibratory cavitation device

A vibratory cavitation device is used for the generation of cavitation in liquid sodium. This device is used for the study of erosion damage resistance of materials in the laboratory as it is a relatively simple arrangement compared to other hydrodynamic devices. It consists of a rod (called horn) to the bottom of which the test specimen is mounted. The top of the horn is threaded to the end of an ultrasonic converter-booster assembly while the bottom of the horn is immersed in the liquid in which cavitation is to be produced. A disc at a nodal point in the horn bears against the top of the vessel containing the liquid and seals the liquid from the atmosphere. The horn is vibrated at ultrasonic frequency of 20 kHz using a piezoelectric (or magnetostrictive) crystal and converter /booster arrangement. The mechanical oscillation of the crystal under the influence of the applied electric (magnetic) field is magnified by the booster to which the horn is mechanically fixed. The horn further amplifies the mechanical vibrations and transmits it to the specimen mounted at the other end. The high frequency oscillation of the specimen, which is immersed in the test liquid, generates an acoustic field in the liquid and produces cavitation at the bottom face (which is normal to the direction of oscillation) of the specimen.

Table 4 – Effect of liquid temperature on collapse pressure.

Initial bubble size = 200 μm, Peak to peak = 25 μm, $\left(\frac{dR}{dt}\right)_{t=0} = 0$

Temp ºC (K)	Vel. of soundm/s	Max rad. mm	Min. rad. μm	Jet vel., m/s	Collapse pres MPa
10	0.85	19.8	16	1077	2183
25	1.33	17.9	24	1897	3846
40	1.66	25.7	29	1191	2415
50	1.85	66.5	36	197	398

Table 5 – Comparison of collapse pressures in water and sodium.

Initial bubble size = 200 μm, Peak to peak = 25 μm, $\left(\frac{dR}{dt}\right)_{t=0} = 0$

Liquid	Temp ºC (K)	Vel of sound, m/s	Max rad., mm	Min rad. μm	Jet vel., m/s	Collapse pressure, MPa
Water	20 (293)	1482	1.07	35.2	741	1090
Sodium	400 (673)	2361	1.33	17.9	1897	3846

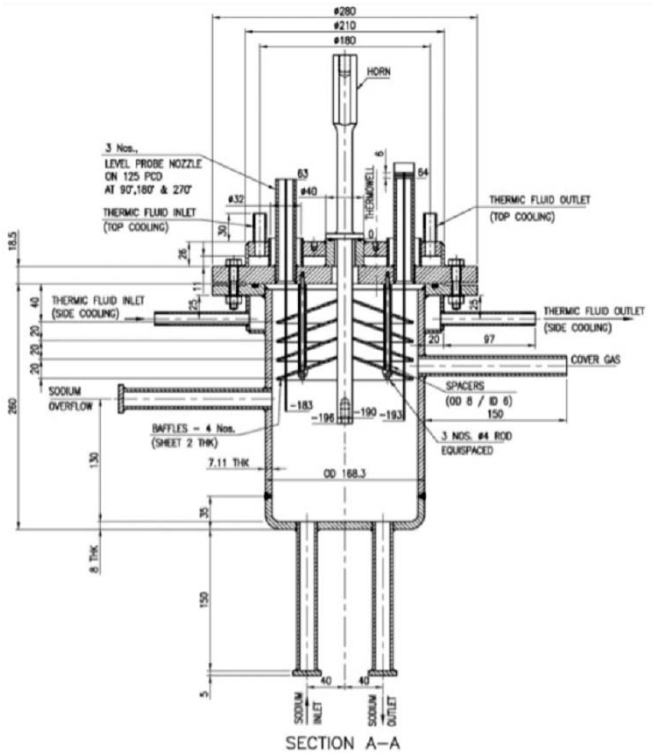

Fig. 5 Cavitation Vessel

Figure 5 is a sketch of the cavitation vessel and horn while Fig. 6 is a photograph of the vibratory test device for in-sodium cavitation damage testing.

Fig. 6 Cavitation equipment for testing in sodium

Results of tests in sodium

Austenitic stainless steel (SS316L) specimens were polished to mirror finished and subjection to cavitation damage testing in sodium using the vibratory device. Figure 7 shows the damage produced in sodium in only 8 min of testing in sodium at 250°C. The intensity of damage produced is indication of the large pressures generated from bubble collapse.

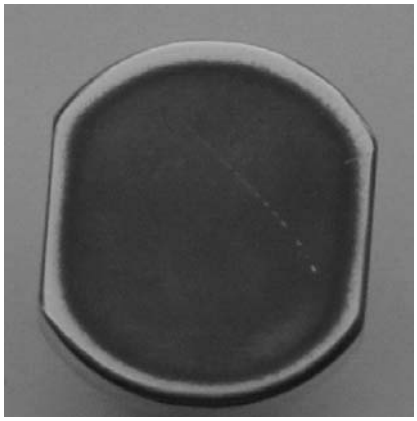

Fig. 7 SS 316 L specimen after 8 min. of testing in sodium at 250ºC

Conclusion

This paper discusses the solution of Gilmore's equation to calculate the pressure intensity resulting from the collapse of a single gas-vapor cavitation bubble. Gilmore's equation is solved for the case of an ultrasonic pressure field and the results of the numerical solution show that the pressures generated from single bubble collapse are large enough to produce damage. The result of cavitation test in sodium at 250ºC using a vibratory device is provided as proof of the severe damage produced due to cavitation.

References

1 **Benjamin T.B.** and **Ellis A.T.,** The collapse of cavitation bubbles and the pressures produced against solid boundaries, *Phil. Trans. R. Soc. Lond. A*, **260** (1966) 221-240.

2 **Rayleigh L.**, On the pressure developed in a liquid during the collapse of a spherical cavity, *Philoso. Mag. Series*, **6** (1917) 94-98.

3 **Plesset M.S.**, The dynamics of cavitation bubbles, *ASME J. Appl. Mech.*, **71**(1949) 277-282.

4 **Noltingk B.E.** and **Neppiras E.A.,** Cavitation produced by ultrasonics, *Proc. Phys. Soc. Sec. B*, **63** (1950) 674-685.

5 **Poritsky H.,** The collapse and growth of a spherical bubble or cavity in a viscous fluid. In Proc. 1st U.S. National Congress on Applied Mechanics (ed. E. Sternberg), New

York, NY: American Society of Mechanical Engineers, (1952) pp. 813–821.

6 **Flynn H.G.,** Physics of acoustic cavitation in liquids, Physical Acoustics, **1B**, W.P. Mason (ed.), Academic Press, New York (1964), Ch. 9, 76.

7 **Herring C.**, Theory of the pulsations of the gas bubble produced by an underwater explosion, in Underwater Explosion Research (Office of Naval Research, Washington, D.C., 1950), **2** (1941) 35–131.

8 **Gilmore F.R,** Growth or collapse of a spherical bubble in a viscous compressible liquids, Hydrodynamics laboratory, California Institute of Technology, (1952), Report no 26-4,

9 **Franc J.P.** and **Michel J.M.**, Fundamentals of Cavitation, Kluwer Academic Publishers, Dordrecht (2004).

10 **Akulichev V.A,** Pulsations of cavitation voids, in: High Intensity Ultrasonic Fields (Ultrasonic Technology), ed. L.D. Rozenberg, *Springer US* (1971), pp 201-259.

11 **Knapp R.T, Daily J.W.** and **Hammitt F.G.**, Cavitation, McGraw Hill, New York, 1970.

12 **Fink J. K.** and **Leibowitz L.**, Thermodynamic and Transport Properties of Sodium Liquid and Vapor, Argonne National Laboratory, U.S. Department of Energy, Oak Ridge, (1995) ANL/RE-95/2.

13 **Ross Macdonald J.**, Some simple isothermal equations of state, *Rev. Mod. Phys.*, **38** (1966) 669-679.

14 **Leighton T.**, The Acoustic Bubble, Academic Press, New York 1997.

15 **Sreedhar B.K, Albert S.K.** and **Pandit A.B.,** Cavitation damage: Theory and measurements – A review, Wear, **372-373** (2017) 177-196.

PhD Thesis Summary

Thermodynamic Study of Some Tannins Using Ultrasonic Measurements

(Awarded To Dr. Ganesh M. Jamankar by Anand Niketan College, Anandwan Warora, Gondwana University, Gadchiroli 2017)

This thesis deals with thermodynamic study of binary liquid mixture of some tannins like Gallic acid, Tannic acid and Ellagic acid with ethanol and acetone at 2 MHz and 4 MHz over the entire range of composition and at temperatures 298K, 303K, 308K and 313K.

The studies of molecular interactions due to structural changes have been explained in this thesis. Measurement of ultrasonic velocity, density and viscosity of binary liquid mixture provides information regarding to their volume, elastic properties and complex formation.

Derived thermo acoustical parameters like adiabatic compressibility, free length, free volume, internal pressure, relaxation time, acoustic impedance, Gibb's free energy, classical absorption, van der Waal's constants, Rao constant, Wada constant, reduced volume, isothermal compressibility, isothermal bulk modulus, molar volume, latent heat, volume expansivity and relative association were successfully employed to explain different types of molecular interactions such as strong, weak, hydrogen bonding, structure making and breaking properties of the interacting components. The work is mainly centered on the understanding of the prevalent molecular interaction in the system. The FTIR technique investigates the possible most favored confirmation of the materials used.

The thesis comprises of seven chapters. Chapter 1 gives brief introduction of the work followed by details of ultrasonic wave production and detection. It also gives the details of propagation of ultrasonic waves through liquids. Chapter 2 comprises the review of literature with sufficient number references related to this study and orientation of present work. The theoratical background, description of the used materials and the methods employed for the study are discussed in Chapter 3. Measurement techniques for the measurements of ultrasonic velocity, density, viscosity, standardization of measurement instruments and computational aspects are discussed in Chapter 4. The results obtained in the ultrasonic velocity, viscosity, density and various thermo-acoustic parameters of the ethanol and acetone based experimental binary systems are presented and discussed in Chapter 5. Chapter 6 contains comparative study of the behavior of the thermo acoustic parameters with FTIR analysis and Chapter 7 gives complete summary and conclusions.

The results of this thesis can be beneficial for the researchers working in the field of medical and material characterization.

Journal of Pure and Applied Ultrasonics

(INDEXED IN: Indian Citation Index, Google Scholar, i-Scholar, UGC)

INFORMATION FOR AUTHORS

1. Type of Contribution

JOURNAL OF PURE AND APPLIED ULTRASONICS welcomes contributions on all aspects of ultrasonics including ultrasonic studies in medical ultrasonics, NDT, underwater, transducers, materials & devices and any other related topic. Contributions should fall into one of the following classes.

Paper - These should be on original research work contributing to scientific developments. They should be written with a wide readership in mind and should emphasize the significance of the work.

Reviews and Articles - Includes critical reviews and survey articles.

Research and Technical notes - These should be short descriptions of new techniques, applications, instruments and components.

Letters to the editor - Letters will be published on points arising out of published articles and papers and on questions of opinion.

Miscellaneous - Miscellaneous contributions such as studies, interpretive and tutorial articles, conference reports and news items are also accepted. Recommended contribution lengths are: Papers 2000-4000 words. Reviews and Surveys 2000-5000 words; Conference Reports 500-1500 words; News Items, Research and Technical Notes up to 1000 words.

2. Manuscripts

Manuscripts should be typed on one side of the paper in double spacing with 25 mm margin on all sides of A4 size paper. A soft copy of the manuscript in MS WORD for text and MS EXCEL for illustrations and a PDF file thereof may be sent by e-mail or CD/ DVD. Colour images should be formatted as JPEG files. Figures submitted in colour would be published in colour. Colour should be avoided unless it is required in order to convey a message or serve a purpose in the image.

Title - Titles should be short and indicate the nature of the contribution.

Abstract - An abstract of 100-200 words should be provided on the title page of paper and review article. This should indicate the full scope of the contribution and include the principal conclusions.

Mathematics - Mathematical expressions should be arranged to occupy the minimum number of lines consistent with clarity e.g., $(x^2+y^2)/(x-y)^{1/2}$.

Illustration - The line illustrations along with captions should be clearly drawn with black Indian ink. Figures in Excel are preferred.

References - References should be referred to in the text by number only. The reference number should be given as superscript. The corresponding reference shall contain the following information in order; names and initials of author (s)(bold), title of the work, journal or book title (italic), volume number (bold), year of publication in brackets, page number, e.g., **Kumar S. and Furuhashi H.,** Anisotropic divergence controlled ultrasonic transmitter array for three dimensional range imaging, *J. Pure Appl. Ultrason.,* **38** (2016) 49-57.

Units and Abbreviations - Authors should use SI units wherever possible.